Review Paper

Accounting for training data error in machine learning applied to Earth observations

Arthur Elmes*[1,2], Hamed Alemohammad[3], Ryan Avery[4], Kelly Caylor[4,5], J. Ronald Eastman[1], Lewis Fishgold[6], Mark A. Friedl[7], Meha Jain[8], Divyani Kohli[9], Juan Carlos Laso Bayas[10], Dalton Lunga[11], Jessica L. McCarty[12], Robert Gilmore Pontius Jr[1], Andrew B. Reinmann[13, 14], John Rogan[1], Lei Song[1], Hristiana Stoynova[13, 14], Su Ye[1], Zhuang-Fang Yi[15], Lyndon Estes*[1] [1]

[1] Graduate School of Geography, Clark University, Worcester, MA 01610, USA; reastman@clarku.edu (J.R.E.); rpontius@clarku.edu (R.G.P.); jrogan@clarku.edu (J.R.); lsong@clarku.edu (L.S.); sye@clarku.edu (S.Y.); lestes@clarku.edu (L.E.)
[2] School for the Environment, University of Massachusetts Boston, Boston, MA 02125, USA; arthur.elmes@umb.edu
[3] Radiant Earth Foundation, San Francisco, CA, 94105, USA; hamed@radiant.earth
[4] Department of Geography, University of California, Santa Barbara, CA 93013, USA; ravery@ucsb.edu
[5] Bren School of Environmental Science and Management, University of California, Santa Barbara, CA 93013, USA; caylor@ucsb.edu
[6] Azavea, Inc., Philadelphia, PA 19123, USA; lfishgold@azavea.com
[7] Department of Earth and Environment, Boston University, Boston, MA 02215; friedl@bu.edu
[8] School for Environment and Sustainability, University of Michigan, Ann Arbor, MI 48109, USA; mehajain@umich.edu
[9] Faculty of Geo-Information Science & Earth Observation (ITC), University of Twente, 7514 AE Enschede, The Netherlands; d.kohli@utwente.nl
[10] Center for Earth Observation and Citizen Science, Ecosystems Services and Management Program, International Institute for Applied Systems Analysis (IIASA), Laxenburg, A-2361, Austria; lasobaya@iiasa.ac.at
[11] National Security Emerging Technologies, Oak Ridge National Laboratory, Oak Ridge, TN 37831, USA; lungadd@ornl.gov
[12] Department of Geography and Geospatial Analysis Center, Miami University, Oxford, OH 45056, USA; mccartjl@MiamiOH.edu
[13] Environmental Science Initiative, Advanced Science Research Center at the Graduate Center of the City University of New York (CUNY), New York, NY 10065, USA; Andrew.Reinmann@asrc.cuny.edu
[14] Department of Geography and Environmental Science, Hunter College, New York, NY 10065, USA; hristiana.stoynova22@myhunter.cuny.edu
[15] Development Seed, Washington, DC 20001, USA; nana@developmentseed.org

*Correspondence: arthur.elmes@umb.edu Tel. 1-304-906-7946 (A.E.); lestes@clarku.edu, Tel. 1-202-431-0496 (L.E.)

This paper is a non-peer-reviewed preprint submitted to EarthArXiv. It has been submitted to MDPI Remote Sensing for peer review.

Abstract: Remote sensing, or Earth Observation (EO), is increasingly used to understand earth system dynamics, in part due to advances in machine learning (ML). ML models typically require large, spatially explicit training datasets to make accurate predictions. Training data (TD) are typically generated by digitizing points or polygons on high spatial resolution imagery, by collecting *in situ* data, or by using pre-existing datasets. TD are often assumed to accurately represent the truth, but in practice almost always have error, stemming from 1) sample design, and 2) sample collection errors. The latter is particularly relevant for image-interpreted TD, an increasingly used method due to its practicality and the increasing training sample size requirements of modern ML algorithms. TD errors can cause substantial errors in the maps created

using ML algorithms, which propagate in derived downstream products. Despite these potential errors and their real-world consequences for map-based decisions, TD error is often not accounted for or reported in EO research. Here we review the current practices for collecting and handling TD. We identify the sources of TD error, and illustrate their impacts using several case studies representing different EO applications (infrastructure mapping, global surface flux estimates, and agricultural monitoring), and provide guidelines for minimizing and accounting for TD errors. To harmonize terminology, we distinguish TD from three other classes of data that should be used to create and assess ML models (training reference data, validation data, and map reference data), but our advice is generally applicable to all four classes. EO researchers should start by determining the tolerable levels of map error and appropriate error metrics. Next, TD error should be minimized through sample design (e.g. by choosing appropriate legend definitions) and during the collection of individual samples (e.g. by using consensus-based collection strategies). We strongly advise that TD error is incorporated in model outputs, either directly in bias and variance estimates or, at a minimum, by documenting the sources and implications of error. TD should be fully documented and made available via an open TD repository, allowing others to replicate and assess its use. To guide researchers in this process, we propose three tiers of TD error accounting standards. Finally, we advise that researchers clearly communicate the magnitude and impacts of TD error on map outputs, with specific consideration given to the likely map audience.

Keywords: training data; machine learning; map accuracy; error propagation;

1. Introduction

Recent technological advancements have led to a new era in Earth Observation (EO, also known as remote sensing), marked by rapid gains in our ability to map and measure features on the Earth's surface such as Land Cover and Land Use (LCLU) [e.g. 1,2], vegetation cover and abundance [3], soil moisture [4], infrastructure [5,6], vegetation phenology [7–9], and land surface temperature [10,11]. The resulting data are used by an expanding set of disciplines to gain new insights into socioeconomic and environmental dynamics, such as community-level poverty rates [12], changes in surface water [13] and forest cover [14], and carbon accounting [15]. As such, EO is increasingly shaping our understanding of how the world works, and how it is changing.

These breakthroughs are facilitated by several technological advances, particularly the increasing availability of moderate (5-30 m), high (1-5m, High Resolution, HR), and Very High Resolution (<1 m) VHR) imagery, as well as new machine learning (ML) algorithms that increasingly require large, high quality training datasets [e.g. 16,17–21]. Training data quality and quantity have a large impact on the accuracy of the maps generated by ML algorithms [22–27], which in turn impacts the veracity of any downstream products based on those maps [28]. While progress in algorithmic performance continues apace, standards regarding the collection and use of training data (hereafter referred to as "TD") remain uncoordinated across researchers [29]. Additionally, much of the research and development of big data and ML is occurring in industry and the fields of computer science and (non-spatial) data science, leaving a potential knowledge gap for EO scientists [30,31].

The measurement and communication of map accuracy is a mature topic in EO and related fields, with a variety of metrics and approaches tailored to different data types, analyses, and user groups [32–40]. However, the impacts of TD error have not been as thoroughly assessed [29], even though such error is almost always present and directly impacts map accuracy [25,26,33,41–43]. Of particular concern is the propagation of errors in further quantitative analyses that rely on ML-generated map products [28]. These derived products are valuable, but potentially magnify errors originating in the initial calibration of the first map [28], illustrating the pernicious effects of unreported error in TD [44]. The problems associated with TD error can be summarized as follows:

1. The 'big data' era vastly increases the demand for TD.
2. ML-generated map products rely heavily on human-generated TD, which in most cases contain error, particularly when developed through image interpretation.

3. Uncertainty in TD is rarely assessed or reported, and TD are often assumed to have perfect accuracy.
4. TD errors may propagate to downstream products in surprising and potentially harmful ways (e.g. leading to bad decisions) and can occur without the map producer and/or map user's knowledge.

These problems suggest an urgent need to review the issues surrounding TD quality and how it impacts ML-generated maps, and to recommend a set of best practices and standards for minimizing and accounting for those errors, which are the primary aims of this paper. Although we focus primarily on TD, our review and recommendations necessarily cover several other data types used to training and evaluating ML models, including reference data, which are often affected by many of the same issues [45]. As such, this paper is complementary to existing work focused on assessing final map accuracy [32–36,39,40]**.**

This paper is organized into three sections. In sections 1 and 2, we present a summary of current practices in the treatment of TD for categorical and continuous map creation, and identify the most common sources and impacts of error and inconsistency. In section 3, we illustrate the impacts of uncertainty in TD generation with case studies that span a range of typical EO applications, including building and road mapping, global surface flux estimates, and mapping agricultural systems. In section 4, we propose guidelines for i) best practices in collecting and using TD, which include defining acceptable accuracy levels, ii) minimizing TD errors associated with training sample design error and collection, iii) characterizing and incorporating TD error in final map outputs, and iv) communicating TD error in scientific and public documentation.

1.1 Current Trends in Training Data Collection

A large proportion of remote sensing projects make some use of TD, typically created either using geolocated *in situ* data [41,46], by visually interpreting high and/or very high spatial resolution imagery [47–49], or by interpreting the images to be classified/modeled themselves [e.g. 50,51,52]. Of these collection methods, image interpretation is increasingly common [53], particularly with the rise in crowdsourcing initiatives [20,54]. As such, mapping is strongly constrained by the creation of TD, which are often treated as absolute 'truth' [45], if for no other reason than that their accuracy is assumed to be perfect [33,42,55]. However, multiple sources of error are possible and indeed likely in TD, whether collected *in situ* or via image interpretation [46].

The use of large, data-intensive ML algorithms continues to grow in many fields, including remote sensing. Neural Networks (NN) are an increasingly used class of ML algorithms, and have seen development into more complex NNs such as Convolutional Neural Networks (CNN), which are able to leverage spatial context to identify objects with distinctive shapes, and which therefore benefit strongly from high or very high spatial resolution imagery [56]. While some forms of ML can function effectively with smaller training datasets, the quality of these data is nevertheless critically important [23]. Additionally, the increasingly popular large-scale, high complexity NNs require substantially more TD than traditional statistical models, and like many ML approaches are sensitive to noisy and biased data, producing the logistical difficulty of creating very large, 'clean' training datasets [57–59].

Partially to address this need, several recent efforts have been devoted to producing extremely large training datasets that can be used across a wide range of mapping applications, and to serve as comprehensive benchmarks [60,61]. Similarly, a recent trend has emerged in large-scale mapping projects to employ large teams of TD interpreters, often within citizen science campaigns that rely on web-based data creation tools [20,62–64].

1.2 Characterizing Training Data Error

Due to different disciplinary lineages, terminology associated with the various datasets used to train and evaluate map algorithms is sometimes contradictory or distinct. Here we harmonize terminology by defining four distinct types of data: training, validation, training reference, and map reference. ***Training data*** (TD), our primary focus, refers to a sample of observations, typically

consisting of points or polygons, that relate image pixels to semantic labels. ***Validation data*** are typically a random subset of TD that are withheld and used to fit ML model parameters and internally evaluate performance. ***Training reference data*** are expert-defined exemplar observations used to assess TD errors during or after data creation. ***Map reference data*** are completely independent observations used to assess final map accuracy; while these may be collected using many of the same procedures as the other three datasets [45], they have more stringent design protocols and can only be used to assess the final map product, rather than used iteratively in model or map improvement [45]. Map reference data are often referred to as the test set in ML literature [65], but we use the former term to align with the well-established EO map accuracy terminology.

1.2.1 Map Accuracy Reporting Practices

To understand how TD errors can impact map accuracy, it is necessary to first review current practices and standards for measuring and reporting final map accuracy, which are well established in the EO literature [34,35,40,45,66]. While the emphasis of this paper is specifically on TD, as opposed to map reference data, it is necessary to review procedures for accuracy assessment. Sampling protocols for accuracy assessment are more stringent than those for the collection of TD [45], but because both training and map reference data are often collected as part of a single campaign or using the same methods [e.g. 50], the stricter set of procedures should be followed for both. We therefore summarize several important features and best practices for error analysis.

Error analysis compares a mapped variable to a corresponding map reference variable. Map reference data used for accuracy assessment are collected according to sampling and response designs that specify, respectively, the probabilities of inclusion for each location, and the protocol for creating the labeled map reference data [45,67]. Map reference data and TD may both be collected as part of a single larger sample[1], provided there is strict separation between the two datasets. Sampling design, whether simple random, stratified random, or systematic is dependent on application and *a priori* knowledge of the study area, and should be probability-based, such that the inclusion probability of each sample relates to the likelihood of that sample unit being included [34,45,68]. If the observations do not have equal probability of selection, then it is essential to convert the sample data to a confusion matrix (i.e. a square contingency table) that reflects an unbiased estimate for the entire population using methods summarized in Stehman and Foody [45].

Map accuracy is typically assessed using a metric or metrics designed to provide information regarding the correspondence of mapped and reference data. The objective of these metrics is to provide insights into the product's expected best use cases and potential shortcomings. Accuracy metrics vary according to whether the mapped variable is categorical or continuous, with each type of variable having its own foundation for error analysis [69–73]. The confusion matrix is the foundation for categorical variables. Conventionally, the table's rows provide mapped categories and the columns show the matching reference categories, with the diagonal entries showing agreement between the two. The confusion matrix is used to calculate user's accuracy (i.e. the complement of commission error), producer's accuracy (i.e. the complement of omission error), and overall accuracy (i.e. the complement of proportion error) [36]. More details on the interpretation of these values and other aspects of the error matrix are provided in several existing publications [32,34,45,69,74–76].

Several other accuracy measures are also calculated from the error matrix. Most prominent among these is the Kappa Index of Agreement [77], which is widely used in the remote sensing and species distribution modelling literature. However, Kappa varies with class prevalence [78] and can be easily misinterpreted, thus its use is no longer recommended [35]. More recently, a number of additional metrics have started to be more commonly used in EO accuracy analysis, in part due to contributions from other disciplines, such as computer science. Due to differing conventions and objectives within these disciplines, the metrics and terminology relating to error and accuracy are

[1]It is often advantageous to have a separate train sample design, however, as these may be more purposive and targeted to classes of interest [45].

often quite different. To help resolve this confusion, we summarize these metrics and their meanings in Table 1.

Table 1: Summary of commonly used error metrics.

Term	Information Content/Typical Usage	Description
Overall Accuracy	Summary metric combining all class accuracies into a single number	Proportion of correctly classified cases divided by the total of all classified cases
User's Accuracy (a.k.a. Precision)	Metric of the intensity of true positives given the classified category in which the true positives were 'found'. The intensity complement of commission error.	Proportion of correctly classified cases relative to the total number of cases classified into the given category
Kappa Index of Agreement	Single metric for overall accuracy	Used to measure the agreement between mapped and reference categories of a dataset while attempting to correct for agreement that occurs by chance.
Producer's Accuracy (a.k.a. Sensitivity, Recall)	Metric indicating the intensity of true positives given the reference category) The intensity complement of omission error.	True positive rate; ratio of correctly classified cases of a given class to the total true cases of that class
Specificity	Metric for commission error; indicates how well the model avoids false positives	True negative rate; ratio of correctly classified negatives to the sum of true negatives and false positives
True Skill Statistic [78]	Metric that combines sensitivity and specificity while accounting for class prevalence	Sensitivity + Specificity - 1
F1 [79,80]	Combined metric of commission and omission error	Equally weighted harmonic mean of precision and recall
Bias (Mean Bias Error)	Quantifies the average difference between predicted and reference variables	The average error, representing the systematic over- or under-prediction of a continuous variable
Root Mean Square Error/Deviation	Measures a combination of the average error and the variability within the distribution of errors	A potentially misleading metric used to measure disagreement between predicted and reference continuous variables
Mean Absolute Deviation	Measures how far points are from Y=X line	Recommended metric to measure disagreement between predicted and reference continuous variables
Jaccard Index, also called Intersection over Union	Between two discrete/crisp datasets, reports the area of intersection divided by the area of union.	Most commonly used metric to indicate accuracy of object-based classification, which is also called semantic segmentation.

A special and increasingly used type of categorical map is derived from Object-Based Image Analysis (OBIA), in which the output map is classified into polygons representing discrete objects [79]. At present there is no commonly accepted standard for reporting the accuracy of such maps in the remote sensing literature [53], since the optimal set of metrics for polygon accuracy assessment depends on the intended use of the categorical map. For example, edge similarity metrics are useful for assessing the segmentation of individual agricultural fields, whereas area based metrics will fail where multiple objects are frequently mapped as a single object [53]. The Jaccard Index, also called Intersection over Union, is a commonly used benchmark in the computer vision and segmentation literature for evaluating polygon-to-polygon classification accuracies, and has the advantage of being straightforward to calculate and interpret [e.g. 80,81–83]. This and other similar area-based metrics can be used in a remote sensing context, and thus may help to strengthen communication between EO and computer vision researchers. However, we caution that for many mapping goals, these metrics should be complemented by others that account for shape and edge similarity. Perhaps due to these complexities, many existing studies have assessed the accuracy of object-based maps using per-pixel accuracy assessments, which itself is problematic because it involves comparing fundamentally different spatial units [53].

The scatter plot, showing the mapped variable on the y-axis and the reference variable on the x-axis, is the foundation of error analysis for continuous variables. Since any point falling off the 1:1 line indicates deviation from a measurement of the true value, a visual assessment of the plot is an intuitive first step for assessing error in the mapped variable. Several metrics are commonly used to quantify disagreement between mapped and reference variables, including mean deviation, Root Mean Square Error (RMSE; a.k.a. Root Mean Square Deviation, RMSD), and Mean Absolute Deviation (MAD). The use of RMSE may be inappropriate, since it combines MAD with the variation among the deviations, and is frequently misinterpreted as the measurement of average error [84–86]. The Receiver Operating Characteristic (ROC) and the Total Operating Characteristic (TOC) enable analysis of a continuous mapped variable relative to a binary reference variable, for example presence or absence [71,87,88]. The area under this curve (AUC) of an ROC/TOC plot is often used as a single measure of overall accuracy that summarizes numerous thresholds for the continuous variable [88].

Most of the metrics reported above (Table 1) provide useful information for users about map reliability. However, the usefulness of that information depends on the map reference data having higher accuracy than the mapped data, which is an assumption that is often unexamined [29,89]. This tendency is illustrated by Ye et al. [53], who reviewed 209 journal articles focused on object-based image analysis and found that one third gave incomplete information about the sample design and size of their map reference data, let alone any mention of error within the sample. Errors in map reference data can bias the map accuracy assessment [42,90], as well as estimates derived from the confusion matrix, such as land cover class proportions and their standard errors [41]. To correct for such biases caused by map reference error, one can use published procedures for estimating map reference data accuracy [42] and to calculate variance measures for area estimates [41]. These approaches depend on quantifying errors in the map reference data. For the common case of image-interpreted map reference data, this can be achieved by having multiple interpreters create reference polygons and labels for the same locations, and then calculating the level of agreement in their categorical labels [29,45,90,91]. Additionally, knowledge of this uncertainty can be quantitatively incorporated into continuous estimates based on the image interpreted data [41]. *In situ* observations can similarly be used to assess the accuracy of image-interpreted map reference samples [46], although their availability is often limited by cost considerations.

1.2.2 Accuracy Reporting Practices for Training Data

In contrast to the literature on map reference data and its use in accuracy assessment, there appears to be relatively little literature devoted to practices and standards for collecting TD and its potential impacts on maps [29,53]. To gain insight into the level of attention TD receives in EO studies, we

reviewed 30 recent, top-ranked[2] research papers describing land cover mapping studies (identified via keyword search on Google Scholar). This assessment showed that only 2 papers explicitly assessed the quality of the TD used in classification, while 16 made no mention of TD standards at all. Over 75% of these studies used image interpretation, as opposed to *in situ* data, in either training, accuracy assessment, or both. One quarter of these papers used unsupervised classifiers in the processing chain to outline training areas, followed by image interpretation to assign labels to the polygons/pixels. Although only a snapshot, this finding suggests that key details regarding the design and collection of TD (and even map reference data) is lacking in the EO literature.

Moreover, it appears to be even rarer for TD errors to be quantified, let alone their impact on map accuracy assessed, despite the fact that response design (which dictates the collection procedures for such data) is known to influence map quality [41]. In one of the few existing studies to examine this subject, Swan et al. [92] (and see relevant work in [53-54]) show how analyst-generated errors in a building footprint training dataset substantially reduced the precision and recall of the resulting ML model. Given such consequences and the infrequency of reporting, it is evident that current practices regarding the collection and presentation of TD are insufficient for the purposes of systematic, reproducible science.

2. Sources and Impacts of Training Data Error

In the following two sections we describe the common causes of TD error and its potential impacts. In addressing impacts of error, we provide a summary of potential problems, and then two concrete case examples for illustrative purposes. We divide the sources of TD error into those related to sample design and those arising during sample collection, which are the two distinct phases in the TD generation process. We stress that impacts of erroneous TD may be subtle or stark, and may be quite idiosyncratic to a given project.

2.1 Sources of Training Data Error

TD error falls within two general classes: 1) errors stemming from the design of the training sample, including selection of the data source, and 2) errors made when collecting the training sample, including the process of digitizing and labeling points or polygons when interpreting imagery, or collecting field measurements. Below we discuss training data errors arising from each of these classes, bearing in mind that the two classes are non-exclusive.

2.1.1 Design-related errors

Errors associated with TD sampling design primarily relate to failures to adequately represent the spatial-temporal-spectral domains of the features of interest within the imagery input to the ML classifier. This causes a disparity between the distribution of TD compared to the true distribution of the mapped phenomenon in geographic and/or feature space [23–26]. This problem is highly relevant in ML approaches, which learn extremely efficiently from the TD, whether or not it corresponds correctly to the mapped environment [25].

Temporal unrepresentativeness in the TD sample designs is a particular problem due to the prevalence of image interpretation as a source for TD, which arises when obsolete imagery is used as the source for collecting training points or polygons and their associated labels [34,47]. The problem is illustrated is illustrated in Figure 1, which contrasts smallholder fields that are clearly visible in a satellite base map (Bing maps) with ground data collected in 2018. Center pivot fields were installed after the base map imagery was collected, but before ground data collection, creating a temporal mis-match between the base map and the *in situ* data. Labels generated from the base map in this case would introduce substantial error into an ML algorithm classifying more recent imagery. New HR and VHR sensors with more frequent acquisitions [e.g. PlanetScope, 93] can help minimize such temporal gaps for projects that are designed to map present-day conditions (e.g. 2018 land cover),

[2]Based on the Google Scholar search algorithm results. Search performed January, 2019, with terms land cover and land use, including permutations of spelling and punctuation.

but do not solve this problem for mapping projects covering earlier time periods (i.e. before 2016). The same can be said for aerial and Unmanned Aerial Vehicle (UAV) acquisitions, which are typically limited in geographic and temporal extent [94]. While hardcopy historical maps can help supplement temporal data gaps, these data sources come with their own problems, such as errors introduced during scanning and co-registration, and unknown production standards and uncertainties.

Figure 1. An example of potential training data error that can arise when image interpretation is conducted on older imagery. The underlying imagery is from Bing maps, which shows smallholder agricultural fields near Kulpawn, Ghana. The white polygons were collected by a team of mappers (hired by Meridia) on the ground using handheld GPS in 2018. The smallholder fields were replaced by larger center-pivot irrigation fields sometime after the imagery in the base map was collected.

Spatial alignment can be particularly problematic with HR and VHR commercial satellite imagery, which have narrow swath widths and are often tasked (i.e. on-demand acquisitions), resulting in substantially off-nadir view angles and limited temporal coverage for certain locations [47]. Due to large view angles and the lack of adequate digital elevation models, overlapping imagery, or other relevant control points, HR/VHR imagery often does not meet the same orthorectification and geopositioning standards as coarser resolution, government operated satellites [95–97]. When integrating HR/VHR imagery acquired at different azimuth and elevation angles, features such as building roofs show apparent offsets similar to those caused by topography. These offsets are particularly problematic for training repeated mappings of the same features, and/or when using an existing vector dataset such as OpenStreetMap as TD [98–100].

TD collected by interpreting HR/VHR imagery is often coregistered with the coarser resolution imagery used as ML model data. This creates a spatial resolution conflict because the relationship between image objects and pixel size may be different, as objects delineated as spectrally homogenous areas in HR/VHR imagery may be part of mixed pixels in moderate or coarse resolution model imagery. This mis-match is similar to the concept of H-resolution versus L-resolution scene models proposed by Strahler et al. [101]; in H-resolution models, the objects of interest are substantially larger than the pixel size, and vice versa for L-resolution models. The incorporation of mixed pixels may degrade classification model performance, or at least introduce undesired spectral variability within classes [102–104].

Similar spatial resolution and scaling issues must be dealt with in combining *in situ* measurements with satellite observations for continuous variables. Field collected data often cannot practically cover the entire area of a pixel in the model data, especially for moderate or coarse resolution imagery, which potentially induces scaling errors based on the modifiable areal unit problem [105,106]. Spatial representativeness assessments and interpolation methods are used to

limit this problem for operational EO science products [107–110], but this issue is likely to be a source of error for most *in situ* TD samples.

Another design-related problem arises from large-scale data collection initiatives that are becoming increasingly common due to the expanding extent of modern EO analyses [e.g. 111]. These efforts, often conducted via crowdsourcing campaigns, typically enlist citizens to collect data a web-based platform [54, 112–114]. Examples include OpenStreetMap (OSM), Geo-Wiki [54], Collect Earth [115], DIYLandcover [113], and FotoQuest Go [116]. In cases where the resulting data might be purely voluntary [64], the resulting sample may lack spatial representativeness due to uneven geographic contributions [23,117].

2.1.2 Collection-related errors

There are several common forms of error associated with TD collection. The first of these are errors of interpretation, which are mistakes created in the process of manual image interpretation. Manual interpretation of images is a primary source of TD, and often does not provide consistent training labels between interpreters [29,32,90]. Image interpretation may be conducted by people who lack experience in the task or are unfamiliar with the context of the study area. In an uncommonly thorough analysis of error from image interpretation, Powell et al. [90] showed that inter-interpreter agreement was on average 86% but ranged from 46 to 92%, depending on land cover. This research, which relied on trained image interpreters, concluded that transitional land cover classes produce substantial interpretation uncertainty, which is particularly problematic since much land cover mapping effort is directed towards change detection. Another image interpretation approach conducted through an online platform featuring automatic accuracy assessment against training reference data [113] found that average interpreter scores in digitizing crop field boundaries was ~80%, which holds true whether the interpreter mapped several hundred sites or < 50 (Figure 2). Increased image interpretation experience thus does not eliminate labelling error, even when analysts are highly seasoned as in Powell et al. [90]. These findings underscore the need for improved and widely accepted standards for TD creation and vetting using predefined training reference data or inter-interpreter comparisons [41,46,90,91,118].

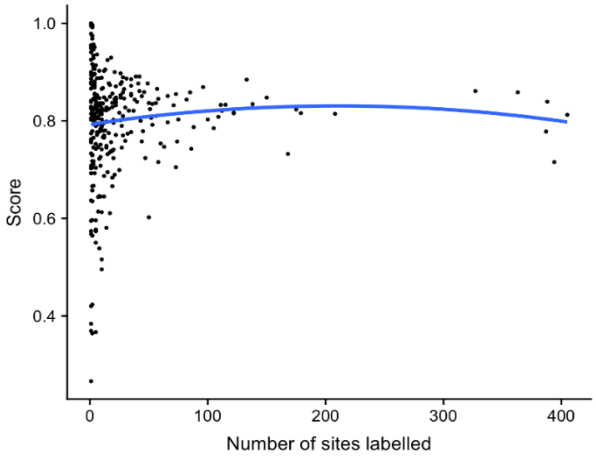

Figure 2: Number of sites mapped per worker versus the average score received at reference sites, where workers' maps were compared to reference maps using a built-in accuracy assessment protocol within a crowdsourcing platform for collect cropland data (Estes et al., 2016).

Labeling error may also results from inadequate or poorly communicated semantic class definitions [119,120], particularly when identifying land use, as opposed to land cover [121]. This is especially evident in urban environments, which are typically spatially and spectrally heterogeneous even within HR/VHR imagery [122]. Critically, such scenes are also semantically vague, even when viewed from ground level. For example, Figure 3 shows a typical example of TD collection for mapping informal settlements (a.k.a slums), in Nairobi, Kenya, in which each of several trained interpreters delineate the same area [123]. Because slums may be defined by sociodemographic factors in addition to spatial and spectral properties, TD creation for such areas is prone to error stemming from semantic issues [120]. Additionally, complex classes such as slums may exhibit high variability between study areas, as local idiosyncrasies link the definition of slums to different physical, remotely observable characteristics. Similar to other target LCLU classes, the

generalizability of informal settlement mapping may be limited, even with local knowledge. These results illustrate the critical importance of TD error analysis and consensus mapping for image interpretation, particularly for heterogeneous target classes with vague or regionally idiosyncratic semantic definitions.

Categorical mapping projects typically define a crisp set of non-overlapping categories, rather than a fuzzy set [124,125]. However, many human and natural land covers exhibit continuous gradation between classes, implying that crisp map legends will necessarily cause semantic ambiguity for TD labels, since many pixels represent a mixture of land cover types [126,127]. This problem is particularly evident with moderate and coarse resolution imagery, which often contain pixels comprising mixtures of the classes of interest [49]. When scene objects approximate the spatial dimension of the image resolution, local variance is highest, leading to poor classification accuracies

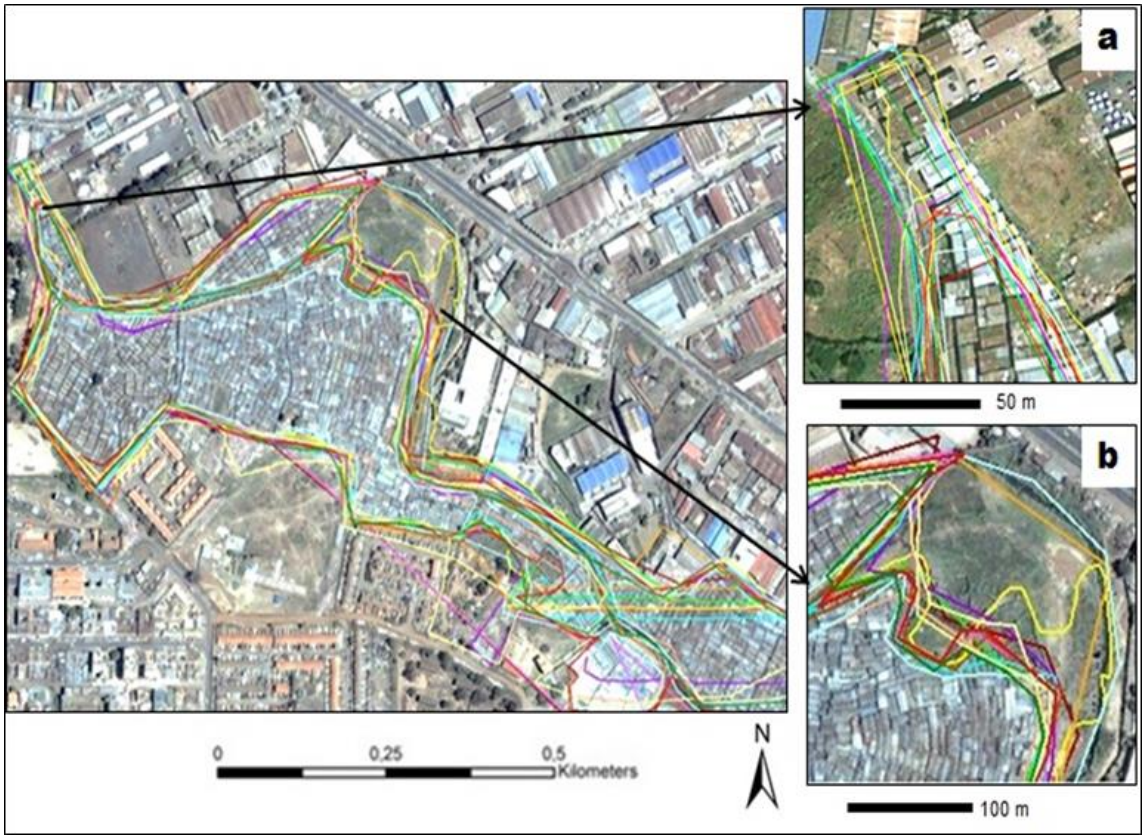

Figure 3: The challenges of mapping slum extent from image interpretation in Nairobi, Kenya. Each colored line indicates a different analyst's delineation of the same slum, illustrating semantic confusion. Adapted with permission from Kohli et al. (2016).

[128]. While substantial research has been devoted to fuzzy set classification and the issue of mixed pixels, crisp categories are still often relied on during the training and testing phases of image classification [129], although Woodcock and Gopal [125] provide a less crisp approach to accuracy assessment. Data errors stemming from unclear class semantic definitions can also be caused by incomplete analyst education prior to data creation, or by poor data creation standards, such as lack of full metadata collection in the field or during digitization [121]. Such inadequacies limit the analysis of TD error, and therefore the ability to account for error propagation.

Collection-related errors may be particularly acute in large-scale crowdsourcing campaigns or citizen science initiatives, in which datasets are often collected rapidly and entail labeling many individual training observations over a short field season or interpretation campaign. In such cases, the balance between speed and quality is a function of interpreter skill, experience, contextual knowledge, personal interest, and motivations for involvement in the data collection [20].

Interpretation errors can be exacerbated when there is insufficient interpreter education or familiarity with the area being mapped, or when contributors lack experience working with EO data and methods. For example, delineation of different classes of urban land use and socioeconomic status may be extremely difficult based only on the spatial and spectral information provided by an image, and without the benefit of local knowledge [120]. Furthermore, participants may have interpret HR/VHR satellite imagery potentially spanning multiple sensors and dates and having varying quality (e.g. cloud cover percentage and atmospheric correction), view/sun angles [130], or image acquisition dates, which complicates interpretation. Inadequate or confusing user interfaces may also lead to error [20,120].

These much larger and cheaper training datasets, often generated by non-expert participants, are increasingly valued for mapping projects. Once these data have been post-processed for noise, they can be highly detailed and spatially extensive [54,57–59]. Nevertheless, quality problems in such datasets can be particularly hard to find and clean, thus representing an important source of TD error that may propagate through ML algorithms and subsequent downstream map outputs [45,114,131]. Therefore, these data should thus be treated quite differently than expert-derived TD.

Errors also arise in *in situ* TD, caused by measurement error, geolocation inaccuracy, incorrect identification of relevant objects (e.g. vegetation species), and other such mistakes [132]. In addition to these factors, some feature types may actually be more difficult to discern on the ground than from an aerial perspective. Aside from these problems, technologically-induced TD errors arise from many and sundry causes, such as mapping or measurement software or hardware defects, user input error, or measurement error in field measurement devices (e.g. spectroradiometer calibration, GPS hardware). However, accounting for quantitative measurement error is more straightforward than thematic TD creation. Textbook tools to quantify measurement error are widely available, and *in situ* data collection procedures often include inter-analyst measurement comparison [133,134].

2.2 Impacts of Training Data Error

TD errors carry through to impact the map production process and outcomes. From a design perspective, the size and class composition of TD is particularly impactful on ML algorithms, which are susceptible to overfitting and class imbalance problems [26,61]. Additionally, the assumption of representativeness of training pixels is often overstated, and many TD may in fact not be generalizable to broader scales (discussed by Tuia et al. [117]).

TD errors also impact map accuracy, which might be particularly pernicious and hard to ascertain when TD errors are unquantified. Studies examining the impacts of TD errors are rare (see section 1.2.2), but some insight into their potential impacts can be inferred from related work. For example, map reference data errors can substantially bias areal estimates of land cover classes, which is problematic for assessment of environmentally or economically important LCLU classes, particularly when examining change [41,89,135]. Similarly, map reference error can bias variance estimation; for example, McRoberts et al. [41] showed that when interpreter error is not included in accuracy assessments, standard errors can be underestimated by a factor of 2.3. While it is possible to quantify error from TD in output maps using the methods of McRoberts et al. [41], the full trajectory of error from initial creation to output map to downstream product has yet to be fully explored.

Further insight into the potential consequences of TD error can be found in studies of map error propagation. For example, Estes et al. [28] examined how error in primary land cover maps transmits to subsequent derived products. This work used a high-quality reference cropland map to quantify the errors in 1 km cropland fractional estimates derived from existing land cover datasets and quantified how these errors propagated in several types of map-based analyses that required cropland fractions as inputs, including estimates of crop production and yield, carbon densities, evapotranspiration, and food security. The results suggest that downstream errors were in some instances (e.g. carbon stock estimates, Figure 4) several fold larger in magnitude than those in the input cropland maps, whereas in other applications (e.g. evapotranspiration estimates), the errors were muted. In either case, the degree to which the error magnifies or reduces in subsequent maps is

hard to anticipate, and the high likelihood that it could have the former effect means that any conclusions based on such land cover-derived maps must be treated with caution if the error propagation is not quantified. This analysis suggests how TD errors might impact the maps they generate, and provides a potential method for quantifying how training errors could impact map accuracy.

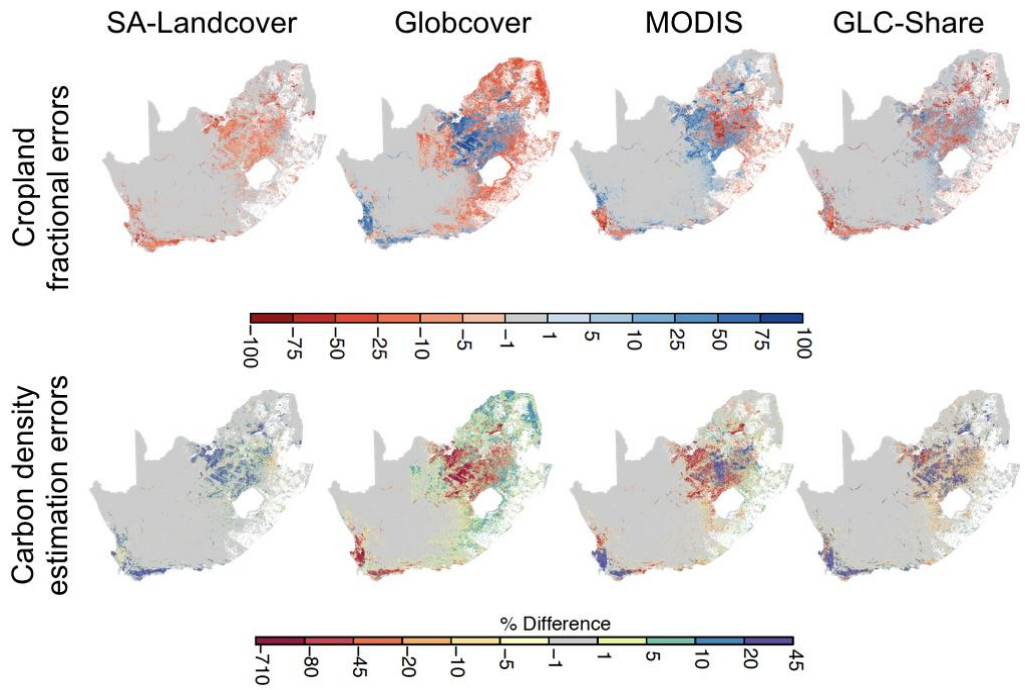

Figure 4: An examination of how error in pixel-wise cropland fractional estimates (expressed as a percentage, top row) can propagate error (expressed as a percentage) in maps that use land cover data as inputs, such as estimates of carbon density (bottom row). Figure adapted from Estes et al., (2018).

Another example illustrating the impact of map input errors is seen in the practice of using well-known standard datasets, such as the National Land Cover Map [NLCD, 136], to map quantities of interest, such as urban tree canopy biomass. Urban trees play a crucial role in regional carbon cycles [137–139], but are often omitted from EO studies of carbon dynamics [e.g., MODIS NPP, 140]. As urban lands are expected to triple between 2000 and 2030 [141,142], there is a pressing need to factor them into carbon accounting, but remotely mapping urban tree cover is limited by a) spatial resolutions that are too coarse for highly variable urban landscapes and b) TD that are often biased to forested, agricultural, and other rural landscapes. For these reasons, the Landsat-derived NLCD Percent Tree Cover (PTC) product [143], which estimates canopy cover at 30-m resolution across the U.S, provides a practical input for empirical models used to map tree biomass. However, previous studies showed uncertainty of this product in urban areas [143], and a tendency to underestimate urban canopy cover compared to a high resolution dataset. Therefore, to quantify the potential impact of NLCD PTC error on canopy biomass estimates, the accuracy of the NLCD PTC dataset was compared to canopy cover estimates derived from manually digitized VHR Imagery for a suburb of Washington, D.C., USA. Results indicated that NLCD PTC underestimated canopy cover by 15.9%, particularly along forest edges (Figure 5) where it underestimated canopy cover by 27%. This discrepancy is particularly important in heterogeneous urban landscapes, where forest edges comprise a high proportion of total forest area. Scaling field data from forest plots to the entire study yielded an estimate of 8,164 Mg C stored in aboveground forest biomass, based on the manually digitized canopy cover map, compared to only 5,960 Mg C based on the NLCD PTC. This finding indicates the significance of these map errors for carbon accounting, as temperate forest carbon

storage and rates of sequestration have been shown to increase by 64% and 89%, respectively, from the forest interior to edge [144]. Quantifying errors in the NLCD is thus important for correcting subsequent estimates trained on these data.

These brief examples help illustrate the potential problems of TD error, but the range of potential impacts is as varied as the number of mapping projects underway across academic research,

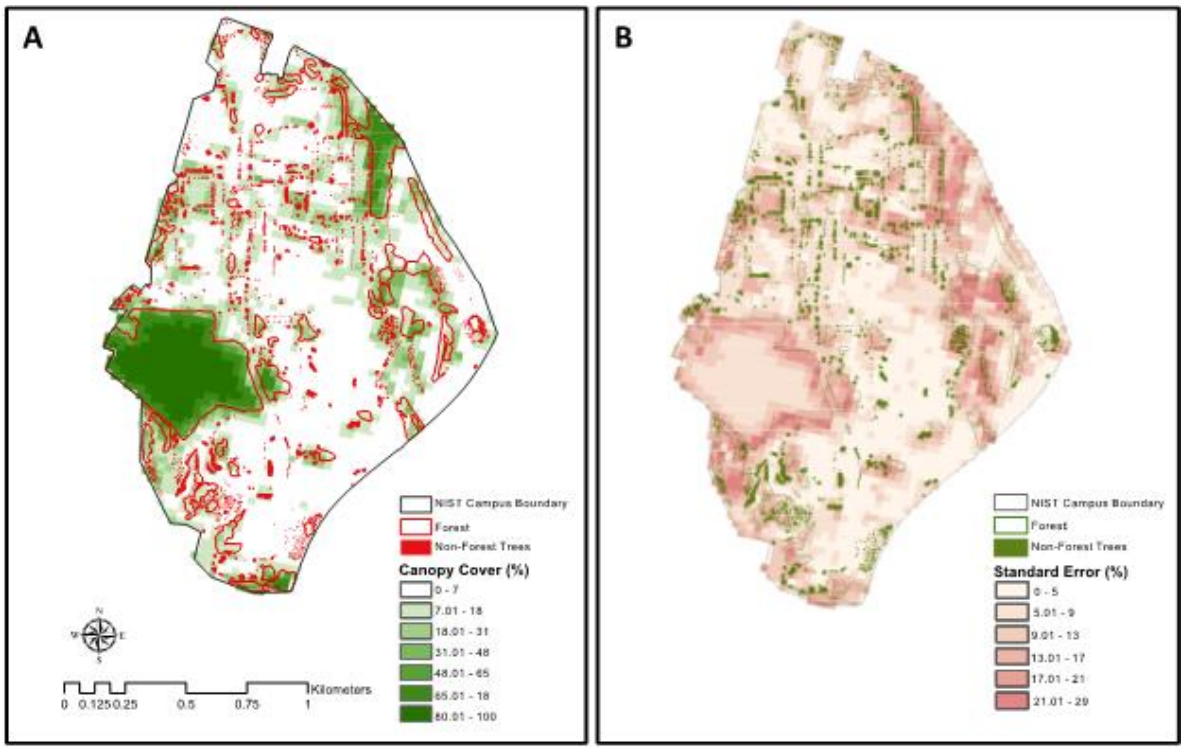

Figure 5: Spatial variations in canopy cover (A) and uncertainty in canopy cover estimates (B) in forested and non-forested areas of the heterogeneous suburban landscape of the National Institute of Standards and Technology campus in Gaithersburg, Maryland. Percent canopy cover at a 30-m resolution from the commonly used National Land Cover Database (NLCD) Percent Canopy Cover product (and its uncertainty) is superimposed over a high-resolution map of forested areas (hollow outlined polygons) and non-forest trees (e.g., street trees; solid polygons) that were manually mapped using <1-m resolution Wayback World Imagery. Note the lower estimates of percent canopy cover along forest edges (A) and the associated higher levels of uncertainty (B) using the NLCD product.

commercial operations, and the public sphere. To represent the growing set of remote sensing applications in which TD error may be encountered, we present a set of case studies below. To help lay a common framework, we show a typical methods sequence for a ML-based remote sensing analysis in Figure 6, which also helps clarify the terminology used in this paper. The figure shows the various sources and implications of error in the modeling and mapping process, beginning with issues in the data sources and sample design, and continuing through model training, validation, and ultimately in map accuracy assessment.

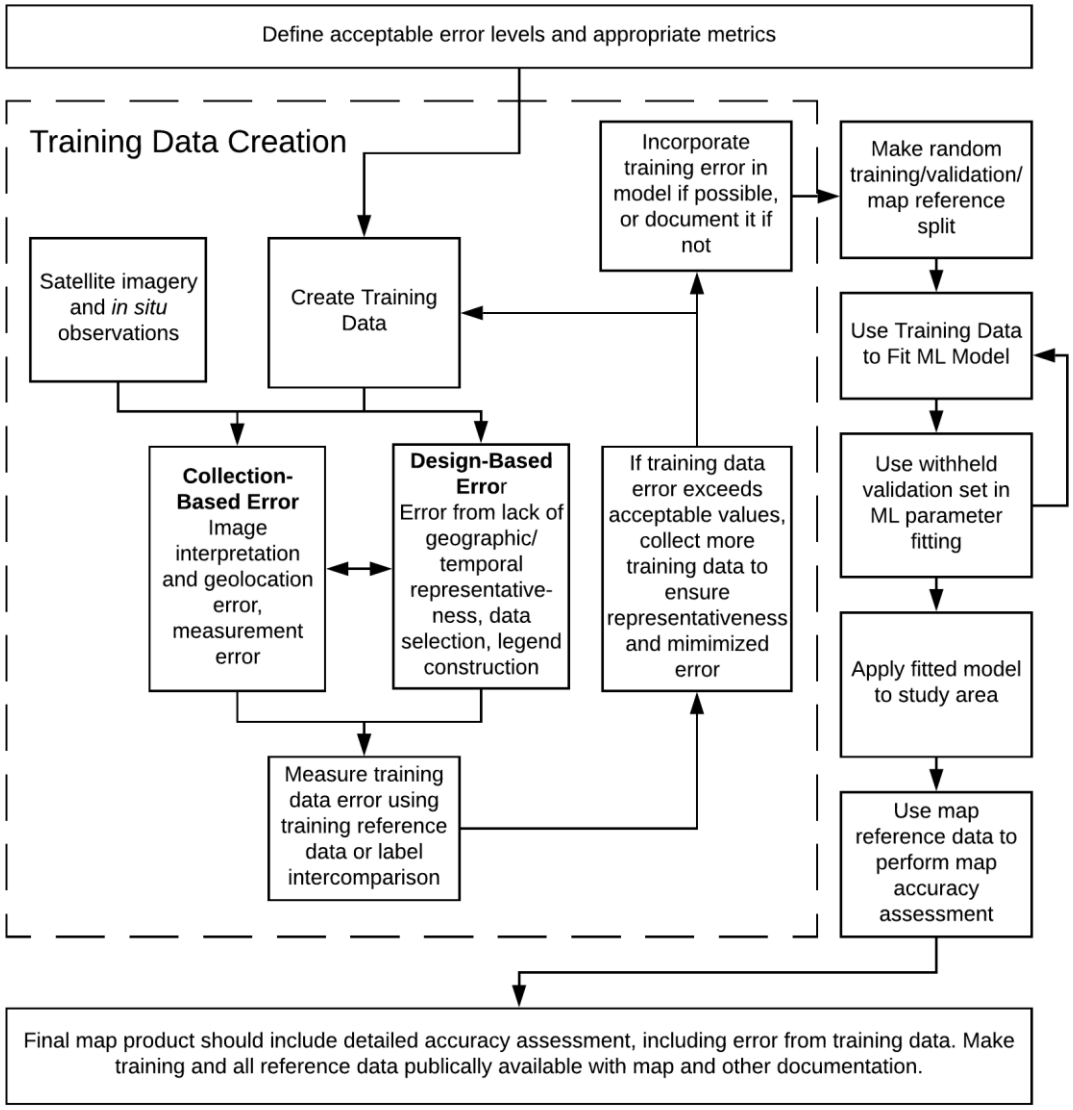

Figure 6: Flow chart of typical workflow for machine learning applications in Earth observation data.

3. Case Studies

To better illustrate the potential impact of TD error, we provide several case studies across different mapping applications that represent the broad range of ML-based mapping and modeling applications that rely on TD.

3.1 Infrastructure Mapping

3.1.1 Incorporating Noisy Training Label Data

Automated building footprint detection is an important but difficult mapping task, potentially benefiting a wide range of applications. The following case study illustrates the use of Raster Vision[3], an open source deep learning framework, to train several models for automated building detection

[3] https://rastervision.io/

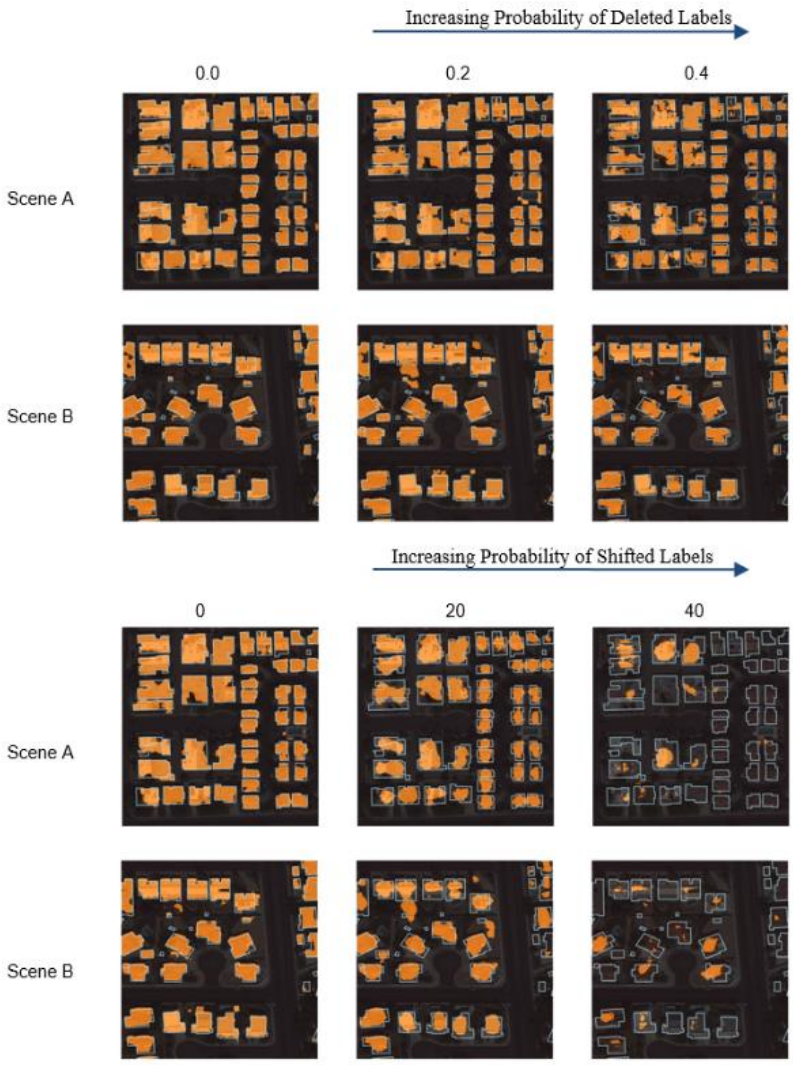

Figure 7: Predictions of the model trained on different noisy datasets. Each row shows a single scene over different noise levels. The top two rows show noisy drops, while the bottom two rows show noisy shifts. The ground truth is outlined in light blue, and the predictions are filled in orange.

from high resolution imagery[4]. These models perform best when trained on a large number of correctly labeled examples, usually generated by a paid team of professional labelers. An alternative, less costly approach was conducted in which a building segmentation model was trained using labels extracted from OpenStreetMap (OSM). However, the labeled training polygons generated from OSM contain errors: some buildings are missing, and others are poorly aligned with the imagery or missing details. This provides a good test case for experimentation on how noise in the labels affects the accuracy of the resulting model.

To measure the relationship between label noise and model accuracy, the amount of label noise was varied while holding all other variables constant. To do this, an off-the-shelf dataset (the SpaceNet Vegas buildings data set) was used in place of OSM, into which label errors were systematically introduced. To this relatively large training data set (~30,000 labeled buildings)[5], missing and imprecisely drawn building errors were systematically introduced, and the resulting model accuracy was measured. The experimental design consisted of two series of six datasets each, with random deletion or shift of buildings at increasing probabilities and magnitudes, respectively. For each dataset, a UNet semantic segmentation model with a ResNet18 backbone was trained using the fastai/PyTorch plugin for Raster Vision[6]. These experiments, including data preparation and visualization, can be replicated using code at[7].

Figure 7 shows the ground truth and predictions for a variety of scenes and noise levels, showing that the quality of the predictions decreases with the noise level. Also, the background and central

[4] Additional detail available at: https://www.azavea.com/blog/2019/08/05/noisy-labels-deep-learning/
[5] https://spacenetchallenge.github.io/datasets/spacenetBuildings-V2summary.html
[6] https://github.com/azavea/raster-vision-fastai-plugin
[7] https://github.com/azavea/raster-vision-experiments/tree/master/noisy_buildings_semseg

portions of buildings tend to be predicted correctly, whereas the outer periphery of buildings presents a greater challenge. These results are quantified in Figure 8, which shows F1, precision, and recall values for each of the noise levels below (see Table 1 for terminology description). The precision falls more slowly than recall (and even increases for noisy drops), which is consistent with the pattern of errors observed in the prediction plots. Pixels that are predicted as building tend to be in the central portion of buildings, leading to high precision.

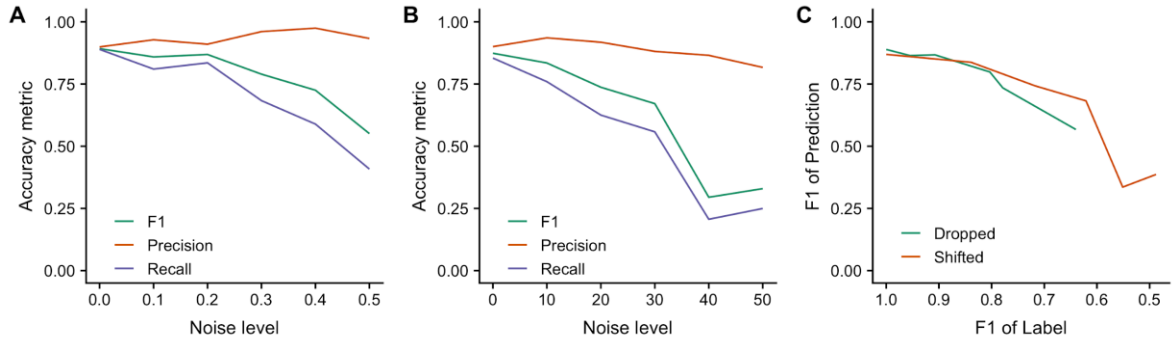

Figure 8: The precision, recall, and F1 scores across different noise levels are shown for the cases in which labels are randomly dropped (A) or randomly shifted (B).

In panels (A) and (B) of Figure 8, the x-axis shows the noise from randomly dropped and randomly shifted labels, respectively. Panel (C) combines the effects of noisy deletions and noisy shifts on accuracy in a single graph, using F1 to measure error. The F1 score of the noisy versus ground truth labels is a function of the pixel-wise errors; this metric has the benefit of measuring the effect of noise on error in a way that is comparable across datasets and object classes. For instance, a noisy shift of 10 in a dataset with large buildings might result in a different proportion of erroneous label pixels than in another dataset with small buildings. From this, it is shown that some of the shifted datasets have a greater level of noise, but that the prediction F1 scores are similar between the two series when the noise level is similar.

These experiments present a small step toward answering the question: how much accuracy is sacrificed by using TD from OSM? Preliminary results indicate, as expected, that accuracy decreases as noise increases and that the model becomes more conservative as the noise level increases, only predicting central portions of buildings. Furthermore, the noisy shift experiments suggest that the relationship between noise level and accuracy is nonlinear. Future work will quantify the functional form of this relationship, and how it varies with the size of the training set. Some preliminary work toward this goal has been described in Rolnick et al. [145], which focuses on image classification of Imagenet-style images.

One limitation of these results is that the magnitude of error in OSM for most areas is unknown, making it difficult to predict the effect of using OSM labels to train models in a generalized, global sense. Noisy error in OSM can be estimated by measuring the disparity between OSM labels to clean labels, such as the SpaceNet labels used in this case, providing a local estimate of OSM noise. A more general but less rigorous approach is to roughly estimate the noise level by visually inspecting the labels in OSM, and comparing to Figure 7, which shows examples of the labels at different noise levels.

3.1.2 Detecting Roads from Satellite Imagery

Road networks constitute a critical geographical data layer used to assist national decision makers in resource allocation, infrastructure planning, vaccination campaigns, and disaster response, among others. However, accurate and up-to-date road networks are not available in many developing countries. High resolution satellite imagery, paired with deep learning methods, provides the capacity to detect and map roads at large spatial scales. This important goal, however, is dependent on availability of local high-quality TD.

To evaluate the impact of local TD availability on predicted road network accuracy, a study was carried out in Kumasi, Ghana [140]. Two datasets were used to train ML models: 1) the SpaceNet[8] Dataset [141] in Khartoum, Sudan, and Las Vegas, USA, and 2) OSM data in Kumasi, Ghana. The SpaceNet Dataset includes high quality road labels with human expert validation, but unfortunately was not available in Kumasi, Ghana. Therefore, the latter study site relied on OSM data, consisting of crowdsourced labels with no accuracy assessment or expert validation. A series of experiments were carried out to assess the feasibility of using transfer learning, using the Raster Vision library in Python for training and evaluation. For all MobileNet V2 models introduced in the following list, the image chip size was set to 300 x 300 pixels, and the training/validation split was 80/20.

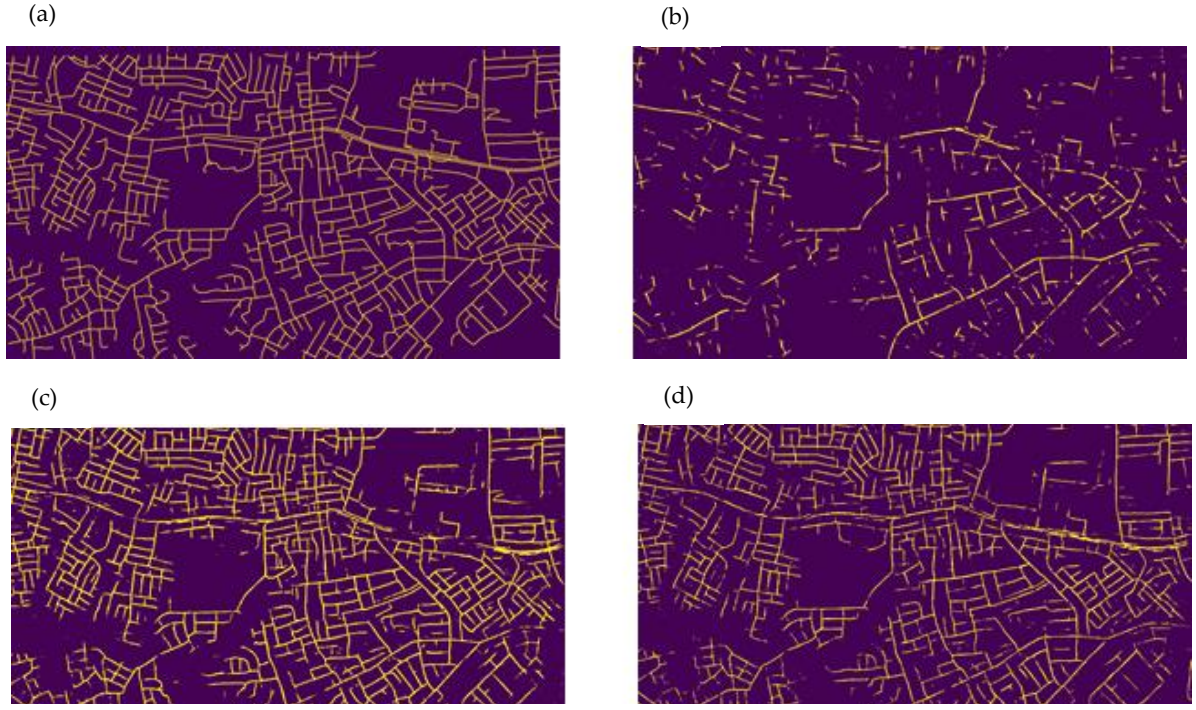

Figure 9: (A) Labels generated by experts for validation. (B) Predictions from the Khartoum Model. (C) Predictions from Kumasi Model. (D) Predictions from Khartoum Model retrained in Kumasi with 10K steps.

The Las Vegas Model was trained and validated on SpaceNet data in Las Vegas and produced very high accuracy predictions. However, when this model was used in Kumasi, it predicted very few roads, with only scattered road segments. The Khartoum Model was also trained using SpaceNet data in Khartoum. The Kumasi Model used Maxar WorldView-3 imagery and labels from OSM as input. OSM was used to test the quality of crowdsourced labels in training a road detection model. The Khartoum Model was then fine-tuned on OSM labels in Kumasi for three different steps of 100K, 50K and 10K. All models used the same hyperparameters, to isolate the role of TD on model performances.

To validate the models' performance using an independent dataset, a set of expert labels were generated over a small part of Kumasi. Figure 9 shows the region with human expert data vetting, along with the three model predictions. The Las Vegas model is excluded from this figure as it does not have any meaningful prediction in Kumasi. Quantitative performance metrics were calculated using the human expert labels, which the models had been blind to during training. The results indicate that, as clearly indicated by Figure 9, the F1 score for roads was substantially higher for the Kumasi Model (0.6458) than when using the Khartoum model (0.3780). However, by retraining and fine-tuning the Khartoum model, the F1 score for roads increased to 0.6135. The full accuracy results for this experiment are presented in Table S1.

[8] https://spacenetchallenge.github.io/

Based on these results, it is concluded that: 1) lack of diverse TD significantly limits the geographic applicability of models, as the types, surfaces, and arrangements of roads varies substantially between regions; 2) regional training datasets are essential for the model to learn the feature of roads in that region; and 3) transfer learning from a reasonably similar geography can help train models.

3.2 Global Surface Flux Estimates

Fluxes at the land-atmosphere boundary play a key role in regulating water, carbon and energy cycles. These fluxes include latent heat flux (LE), sensible heat flux (H), and gross primary production (GPP). While these fluxes cannot be measured directly from remote sensing observations, other remotely sensed variables can be used to estimate these fluxes. Moreover, these three fluxes are highly coupled, and therefore a coupled model is ideal.

A fully connected neural network model was developed for this purpose [142], named Water, Energy, and Carbon with Artificial Neural Networks (WECANN). Inputs to WECANN are remotely sensed estimates of precipitation, soil moisture, net radiation, snow water equivalent, air temperature and solar induced fluorescence (SIF). The target variables for training the model were derived from outputs of global models. However, this presents the difficulty that the target variables are model outputs that can have substantial error, which will propagate in the WECANN model. To mitigate this problem, three independent estimates of each of the three fluxes (LE, H and GPP) were retrieved from the global models. Then a novel statistical approach, named Triple Collocation (TC, Figure S1, equation S1), was used to combine those estimates to a new dataset for training the WECANN model.

Triple collocation (TC) is a technique for estimating the unknown error (measured with standard deviations or RMSEs) of three mutually independent measurement systems, without treating any one system as zero-error 'truth' [143]. The three measurement systems estimate a variable collocated in space and time, hence called Triple Collocation. Using these probabilities, at each pixel and at each time one of the three estimates of the target variable is randomly selected to generate the TD.

The results of WECANN model outputs were evaluated against ground measurements from global FLUXNET towers from 2007 to 2015 (Figure 10), using both the coefficient of determination and Root-Mean-Squared-Error (RMSE) to evaluate accuracy. These show that WECANN's correlation was on average 17% higher (range 8-51%) than that of any one of the three individual inputs, while the RMSE was 21% lower (range 4-54%). These differences provide a partial quantification of the error inherent in any one of these training inputs, and show that by combining them using the TC technique, we can reduce error in an ML model for predicting the fluxes at global scale. This case study illustrates a means of assessing and accounting for error in TD for cases in which these data are not created specifically for the project, but rather are pre-existing data products with potentially quite different characteristics and potentially unknown error.

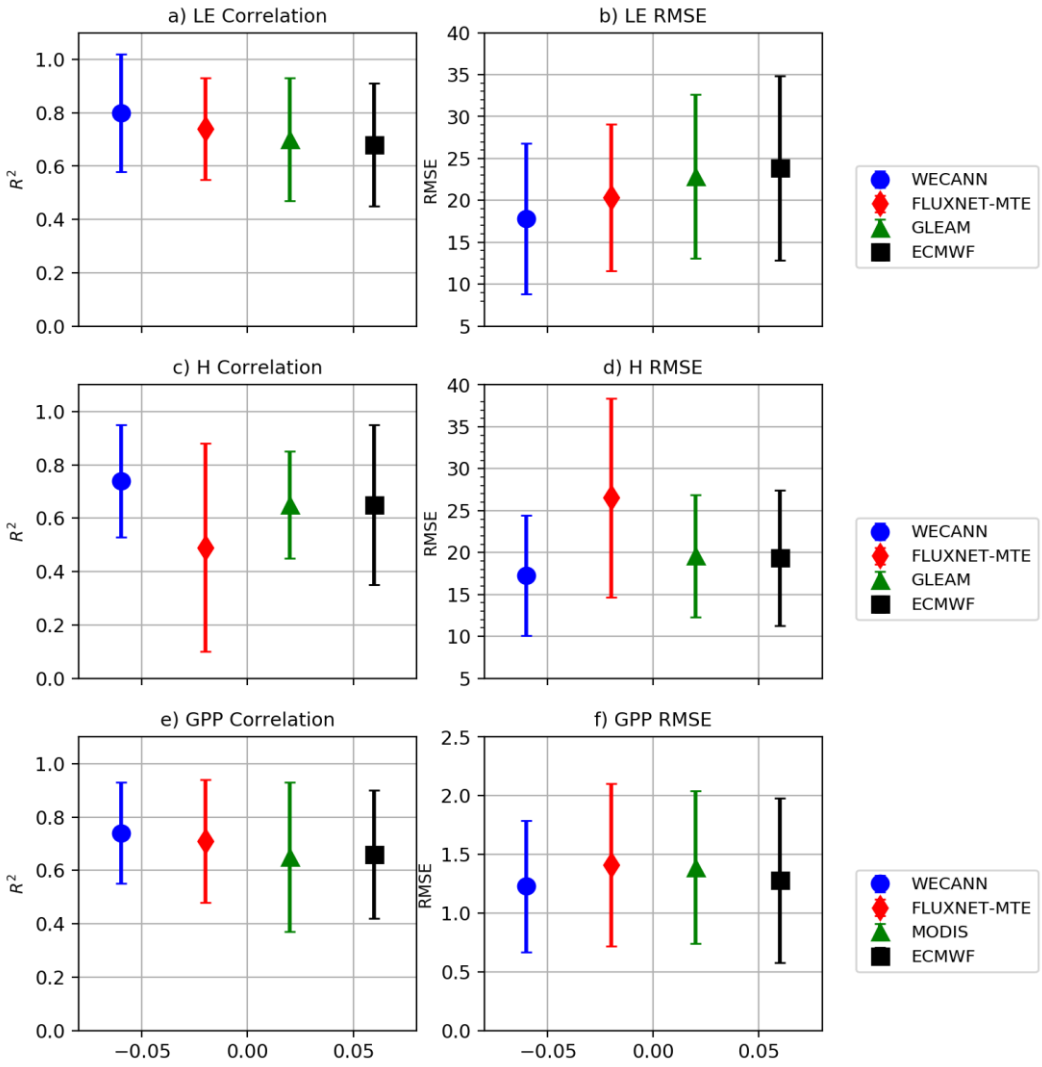

Figure 10: R^2 and RMSE of the WECANN model output against ground measurements from FLUXNET towers in comparison to the three datasets used to generate the target training data for LE (a, b), H (c, d) and GPP (e, f).

3.3 *Agricultural monitoring*

Two agricultural cases illustrate how TD error can impact both categorical and quantitative remotely sensed measures. The first relates to cropland mapping, and is drawn from an ongoing study focused on mapping smallholder agricultural fields at high resolution (3-4 m) in Ghana. The mapping method is based on 'active learning', in which a RandomForest-based [146,147][145] ML algorithm is iteratively trained and validated by a crowdsourcing platform, which enlists human trainers to visually interpret and digitize field boundaries visible within the imagery (PlanetScope visual and near-infrared surface reflectance [93]) being classified [112,113,148]. The crowdsourcing platform incorporates a protocol for assessing the accuracy of training labels, in which each worker is periodically directed to a training reference site where the boundaries are already known but are not visible to the worker. Using these training reference sites, their maps are then scored using a multi-dimensional accuracy assessment algorithm [113], resulting in an average TD accuracy score for each worker that ranges between 0 (complete disagreement with reference) and 1 (perfect agreement). Each label site is mapped by at least five workers, and the resulting worker-specific accuracy scores are used within a Bayesian merging algorithm to combine the five sets of labels into a single consensus label, which is then used to train the RandomForest classifier. Here we use the worker-specific training accuracy scores to assess the impact of label quality on map accuracy, by

assessing three variants of two RandomForest-generated maps, one over Central Ghana (~3,400 km^2) and one over Northern Ghana (~3,100 km^2). The first two maps were trained using labels generated by the least accurate worker to map each training site, the second two by the most accurate worker to map each site, and the third using the consensus labels. The accuracy of each pair of maps was then assessed against the validation set (reserved consensus labels) using the True Skill Statistic [78] (sensitivity + specificity - 1, with scores ranging from -1 to 1). The results show a substantial difference in accuracy between the maps trained with the least and most accurate workers' labels (Figure 11A), with the former having 7-9% more skill than the latter, while maps based on consensus labels have ~3% more skill than those of the most accurate workers' labels.

The second case relates to remotely sensed crop estimates of wheat yields collected in 48 smallholder fields in Bihar, India in 2016-17 [149]. Yield data were collected via eight 2x1 m^2 crop cuts within each field, and PlanetScope-derived green chlorophyll vegetation indices (GCVI) were calculated over each field from imagery collected over four dates during the growing season (January 13, February 25, March 12, and April 14, 2017). A RandomForest regression was trained on the yield measured for each field, using the four dates of GCVI values as predictors. To test the effect of TD error on the resulting yield predictions, three types of noise were artificially introduced into the yield

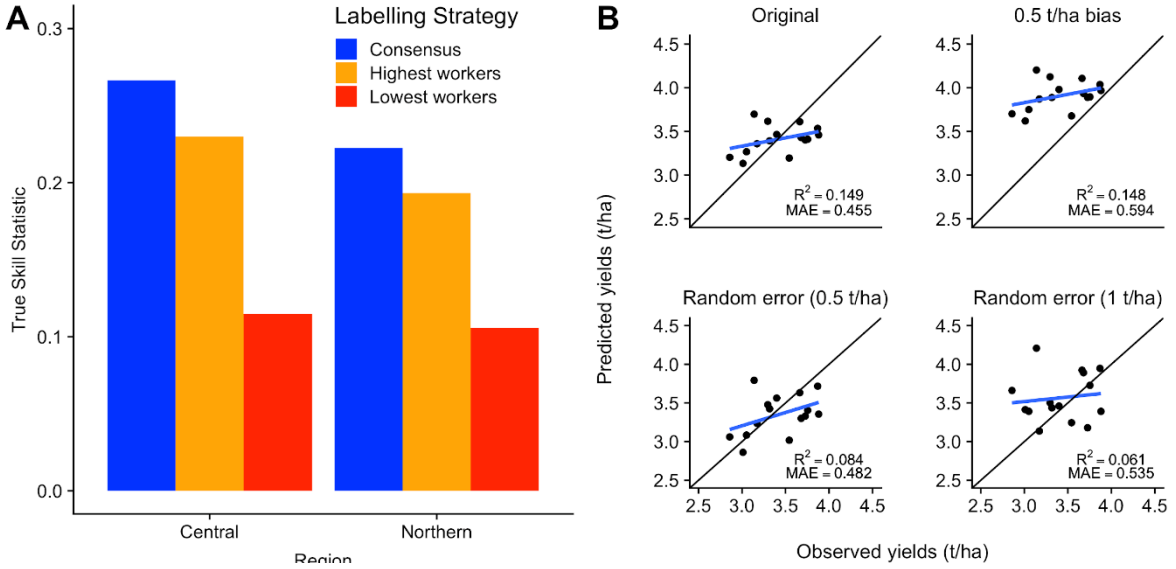

Figure 11. A comparison (A) of the accuracy (based on the True Skill Statistic) of cropland maps over two areas of Ghana when generated by labels of different levels of quality (red = least accurate workers' labels; orange = most accurate workers' labels; blue = "consensus" labels made by merging all workers' labels). (B) Results from a RandomForest model of wheat yields trained on satellite-derived vegetation indices, showing the relationship between predicted yield and independent observed yields, in terms of the fit against the 1:1 line and the regression slope of the relationship (points and regression line represent the mean of a single randomly selected model permutation). The average mean absolute error (MAE) and average regression R^2s calculated across all permutations are shown for each model.

data used for training: 1) a systematic 0.5 ton/ha overestimate, and randomly distributed errors sampled from a normal distribution with a mean of 0 ton/ha and 2) standard deviations of 0.5 ton/ha and 3) 1 ton/ha. A baseline model fit to unperturbed data was also developed. Each model was trained on three separate randomly selected subsets of 32 perturbed observations, and the predictions were made for the remaining 16 held-out (independent) yield observations, which were not perturbed. This three-fold cross validation process was repeated 50 times, with each permutation using a different random seed to construct the folds, in order to achieve stable error metrics. The model performance was assessed by calculating the averages of the mean absolute error (MAE) of the prediction, and the R^2 of regressions fit between prediction and observed values (Figure 11B).

The results show that four models, including the baseline, compressed the range of yields, as seen in the shallow slope between observed versus predicted values, but prediction error was 18-31% higher when training yields had either the high level of random or systematic error within them. The smaller amount of random noise only added about 6% error to the predictions, suggesting that RandomForest is tolerant to some training error. Note that the average R^2 of the observed-predicted regression fit was nearly the same for the systematic error case as the baseline, which shows that this metric can be an unreliable measure of performance for quantitative measures, and that it is important to assess fit against the 1:1 line and using a metric such as mean absolute error.

4. Guidelines and Recommendations

Although our review and case studies show that impacts of TD error on EO applications can vary, and that the existing literature on this problem is scarce, several best practices and guidelines emerge from this work. Below we outline a series of suggested steps for minimizing and accounting for TD error, within the context of undertaking and assessing the accuracy of a typical ML-based mapping project.

Step 1: Define acceptable level of accuracy and choose appropriate metric

As a starting point, analysts and map-makers should first determine the level of error that is tolerable for their particular application, and then determine the metrics that are best suited for assessing map accuracy within the context of the research questions or hypotheses [150]. For example, if the goal is to estimate the number of hectares of a category, then commission and omission errors of that category cancel each other out, and therefore the gross error for the category is less relevant than the net error for the category [35]. In the case of a continuous variable, in which the absolute accuracy of the mapped value is of greatest importance (e.g. for predicting grain yields in different areas), assessing the fit of the relationship between predicted and observed values along the 1:1 line is important, together with measures such as mean absolute error and mean error [85,86].

It is important to emphasize that the ability to determine tolerable map error is limited by the extent to which the amount of error in the *map reference data* is known. The error in these data determine the upper limit of achievable map accuracy, since a model's predictions cannot be more accurate than its map reference data (or if they are, then that cannot be known). Put more simply, if the map reference data are only 90% accurate, then the map can be said to be at most 90% accurate. While this may seem intuitive, it is often not sufficiently considered, since map reference data accuracy is often assumed to be perfect [33,42,55], when in fact, as with TD, there is always likely to be some error. Map reference data error has two important ramifications. First, if the map reference data error is greater than the tolerable error level, then there is little point in attempting to improve the map algorithm, unless a different reference dataset with tolerable error can be obtained. Second, if the error in the map reference data is unknown, then it is impossible to properly assess map accuracy, including how accuracy is impacted by TD error.

Although the aforementioned considerations relate to map reference data, they are highly relevant to and intertwined with TD. Training and reference data are often affected by the same sources of error, particularly when both datasets are generated simultaneously using the same methods, which is common practice [50,112]. The procedures for minimizing and accounting for errors in both datasets are thus often the same. Our subsequent recommendations therefore cover both training and map reference datasets, except where we indicate necessary distinctions. Furthermore, the method we recommend for assessing TD label uncertainty may also provide the most practical and effective method for assessing accuracy in many reference datasets (see section 1.2).

Step 2: Minimize design-related errors

The next logical step in a mapping project is to design a strategy for collecting the training and map reference samples. Although there are numerous factors to consider, there are several general aspects of design that can help minimize potential training errors.

Sample design

The first of these relates to sampling design itself, i.e. where, when, how many, and what type of samples are placed. With respect to the TD, to a certain extent this depends on the requirements of the selected ML algorithm, which can have differing requirements with respect to class balance [e.g. 26]. However, one critical design aspect relates to cases where training and reference samples are generated simultaneously. In these cases, it is essential that considerations of the TD sample not undermine the standards required for an independent, probabilistic map reference sample [55]. These standards are not necessarily violated when both training and reference samples are generated by the same people [45]. Instead, the potential for error arises if iterative refinement of the algorithm is done against the map reference dataset. This problem can best be understood within the context of cross validation, which is appropriate for ML parameter selection [e.g. 26], but when the number of folds exceeds one (as in our yield estimation case study; Figure 11B) then the portions excluded from training lose statistical independence and can no longer serve as the map reference for the purposes of ascertaining final map accuracy [65]. However, the risk of losing map reference data independence may also occur when training sites are selected iteratively, in order to increase their representativeness and improve ML performance [50,112]. If the performance gain due to new training sites is assessed against the map reference, then it will also lose independence after the first iteration. Moreover, any error in the map reference sample will be integrated into the final map. Xiong et al. [50] avoided this problem by assessing performance gains from additional training data through visual assessment of their ML-generated cropland maps against other similar land cover products. A more quantitative approach is to divide an initial sample into three splits: one for training, the second for validation for algorithm improvements, including those related to the addition of new training sites, and the third as the map reference, used only for final accuracy assessment. This partitioning approach can be implemented in the mapping platform used in the cropland mapping case study [Figure 11A, 147].

Geographic representativeness and the degree to which TD capture the variability in the feature of interest is an important sample design consideration [113,151]. The road mapping case study shows the errors that can result when maps are trained with samples that do not adequately represent the features in a geographic region. Training data can in practice be highly localized or relevant for a limited spatial extent or temporal period [120,152]. This problem may become more relevant given the increase in stock or benchmark training libraries, and attempts to transfer pre-trained models to other regions, time periods, or scales of observation [61,153]. Such training libraries can present an immense benefit to large extent EO research, but if these are to be relied on for training, their representativeness of the features of interest should be assessed, and augmented as needed, as in the Khartoum model case study (Figure 9D). However, we suggest that the best practice is to train using data specifically collected within a bounded region for the feature being mapped [e.g. within a particular agroecoregion, 50,154], and avoid over-generalizing or transferring models to other regions [155]. When using citizen science or crowdsourcing approaches to generate these data, representativeness is ensured by directing labelers to the selected TD sites [e.g. 113], rather than having them select regions to map.

Samples should also be temporally representative of the imagery that is being classified. That is, relative to the imagery being classified, the training (and map reference) sample should fall within a window of time that matches the characteristic rate of change of the feature being mapped. This temporal interval can be estimated by assessing the temporal autocorrelation in the feature of interest [156]. For rapidly changing features, such as the timing of deforestation events, snow/ice melt, and vegetation coverage during phenological transition, the sample may need to be captured within a few days or weeks of the acquisition of the imagery being classified, whereas for slower-moving features a sample collected within a few years may be sufficient.

Training Data Sources

The requirements for temporal representativeness make the source of training imagery a critical consideration for projects that rely on image interpretation. The use of basemap imagery is not recommended for training when mapping dynamic features, given the broad range and uneven distribution of image ages in these basemaps [47], unless the age of the imagery being classified can be matched to that of the training sample. Otherwise, there is substantial potential for introducing error into the algorithm (e.g. Figure 1), and its impact may be hard to assess, particularly if the reference sample was also collected from the basemap. The goal of temporal representativeness must be balanced with the need to have a sufficiently high spatial resolution for accurate image interpretation, which helps minimize errors during the collection of the sample (see Step 3). Beyond matters of cost, this tradeoff is presumably one reason why HR/VHR basemaps are widely used [47]. New commercial imagery, such as PlanetScope [93], which are collected at high temporal frequency (near-daily) with a sufficient spatial resolution (3-4 m) for many visual interpretation tasks, may be a preferable source of training imagery for developing maps that represent the post-2016 period.

It is also important to consider and account for additional sensor and imagery characteristics that shape interpreter data entry, such as spatial resolution, atmospheric quality (e.g. clouds, haze), sensor view angle, sun angle, spectral band selection, and image rendering contrast stretches. These characteristics should be taken into consideration in the sample design stage, although this information may not be available to obtain *a priori* [62].

Legend design

For thematic maps, legend design merits special consideration as it relates to TD, particularly for multi-temporal and/or large area projects that rely on multiple image datasets [47]. Objects of interest, including land cover types, should be at least twice as large as the pixel resolution of the imagery used in the classification algorithm [101,128,157]. When image spatial resolution is too coarse relative to the scene elements of interest, image interpretation errors are likely due to mixed pixels [102–104]. This implies that in designing a legend, researchers should select classes that can be effectively mapped using the coarsest resolution imagery that will be incorporated in the model to avoid the problem of collecting training samples with mixed pixels. This is especially relevant since HR/VHR imagery is often used to create training polygons and labels, while moderate or coarse resolution imagery is most often used in model processing [e.g. 50,158–160].

Continuous TD, particularly those collected *in situ*, are often point samples, and therefore a sampling protocol should be used to match field measurements and pixel dimensions in order to avoid scaling problems associated with the modifiable areal unit problem [105,106]. Spatial representativeness should be considered as a limiting factor for legend design, and to the extent possible, researchers should attempt to use categories that are supported by both the spatial resolution of the model data and the field sampling protocols to be used [107–110].

Step 3: Minimize collection-related errors

There are numerous ways to collect TD for categorical and continuous mapping projects, each with their own sources of error. There are therefore many potential approaches for minimizing associated collection errors, which in many cases may be relevant only to a particular variable [e.g. for agricultural area estimates 161]. Practices for controlling measurement errors in continuous variables are often well understood and part of conventional field data collection practices. We thus focus primarily on strategies to minimize error in image interpretation, an increasingly common practice used for training categorical mapping algorithms. We also touch on the specific case of model-derived training data.

Beyond the design considerations mentioned above, there are several steps that can be taken to minimize error during the collection of the training sample. Whenever possible, we recommend using built-in accuracy assessment protocols, particularly for image interpretation [113]. For example, active feedback during training label creation can help reduce errors on a rolling basis, by providing

interpreters information regarding their performance [162]. This strategy relies on predefined training reference data for comparison with interpreter-generated labels. Training reference datasets can be limited in size compared to the ultimate sample size, provided that training reference locations are randomly presented to interpreters during the data creation campaign [113].

Since absolute truth is an impossible standard, consensus among domain expert interpreters can be used as the best and most practical measure of 'truth' for the training and map reference data [29,45]. McRoberts et al. [41] showed that an increased number of interpreters reduces bias in the estimated variable. Since this is the only readily controlled factor during image interpretation campaigns, these authors recommend at least three image interpreters be used, such that at minimum a majority vote interpretation rule be possible. For cases when land cover proportions are unequal, estimated bias was shown to be larger, and thus as many as seven interpreters are recommended in those cases. In the cropland mapping case study, five interpreters were used per site. As illustrated by the agricultural and surface flux case studies, methods involving multiple independent measurements at the same location provide a mechanism for assessing TD uncertainty (Figure 12), in addition to minimizing error during creation. In the case of image interpretation, this involves multiple interpreters assessing the same site, similar to *in situ* methods in which multiple analysts independently make the same measurement of a continuous variable.

In any case, image interpreters should be given thorough instruction regarding remote sensing principles as well as local or regional contextual information. Analysts with local domain expertise are particularly helpful in consistent identification of idiosyncratic land covers [123]. Our recommendations regarding interpreter education are particularly relevant for crowdsourcing or citizen science data collection campaigns, in which it cannot be assumed that participants have any formal experience in image interpretation.

As described above, image interpretation is inadvisable in cases where the available imagery does not support the legend categories, or the similar but potentially more hazardous case that HR/VHR imagery is used to create training samples that are then used with coarser resolution imagery when ingested into the ML model [see 101]. Assuming that researchers correctly specify their data selection and legend design, image interpretation errors due to insufficient resolution should be minimized; however, special care should be given to borderline classes, or classes exhibiting a high degree of spatial and/or spectral variability due to land cover mixtures within the pixel [102–104,117]. In such cases, we recommend that training protocols include the practice of leaving a buffer around training polygons whose pixels may be mixed over relatively small distances, as described by Xiong et al. [50].

It is also possible to generate TD for maps of continuous variables using process-based simulation models. A prominent example of this approach is seen with crop yield mapping, where field-estimates of yield are hard to obtain and can have substantial error [163]. One particular example is the Scalable Yield Mapping (SCYM) method [164,165], in which a mechanistic crop model is used to simulate yield under a large number of various environmental and management conditions. The crop model's outputs then become inputs for training an empirical model (typically ML) that uses a subset of the model variables that are remotely retrievable as predictors. The yields are then mapped using the empirical model. TD errors in such cases can be minimized by rigorously calibrating models (itself a challenging task) according to best practices from the relevant modeling literature, such as those recommended for crop simulation [e.g. 166]. Alternatively, if modeled TD are necessary but careful calibration is not possible (e.g. because the data are pre-existing), then a merging approach such as Triple Collocation (Section 4.2) may be employed to reduce training error.

Step 4. Assess training data error

The best way to assess TD error is to measure it directly. For continuous variables, calculating measurement error should be possible in many cases, even for model-generated TD, in which the variance can be calculated from simulation treatments [e.g. 166]. For categorical mapping, training error can be measured using an internal accuracy assessment protocol that makes use of predefined training reference data (e.g. Estes et al., [113]). During TD creation, whether *in situ* or via image

interpretation, we recommend calculating quality metrics for the data creators, relating to speed, precision, and consistency. This recommendation is based on experience in crowdsourced data creation [113,114], but it is applicable to any type of data collection, and could greatly bolster the understanding and quantification of error propagation. However, it can be challenging to produce training and map reference data [33,34,41,76], and indeed in some cases the true category is not clear, whether looking at an image or standing on the ground in the same location. When target land cover classes are vague or difficult to delineate, local knowledge can help compensate for difficulties in image interpretation (Figure 3). At the minimum, we recommend reporting the percentage of the reference observations for which the category is ambiguous.

If an accuracy protocol including pre-defined training reference observations is not possible, then we recommend that researchers calculate uncertainty estimates based on repeated measures approaches, as described above and shown in Figure 12; this is useful for both training and map reference data. If no quantification of TD error is possible, then researchers should at the very least clearly document the data creation methods, and detail likely sources of error and potential uncertainties.

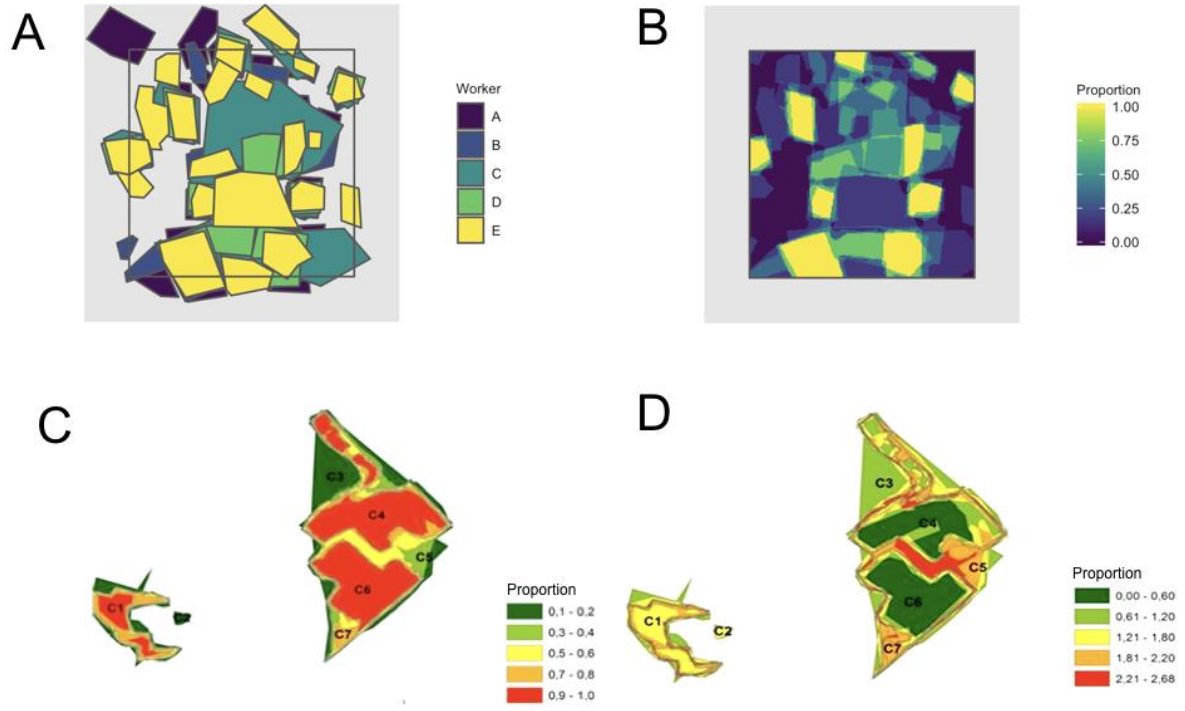

Figure 12: Two examples of consensus-based mapping approaches and their potential use for assessing training (or reference) data uncertainty. Panel A shows a collection of crop field boundary polygons drawn by five independent workers around crop fields visible in PlanetScope imagery collected over Ghana. These labels can be converted into a heat map (B) showing the overall agreement, the inverse of uncertainty. Similarly, 19 independent experts were asked to delineate slum settlements in image subset from Cape Town, South Africa. The polygons are converted into overall agreement and the uncertainty is modeled using random sets (C) shows the covering function, which is then used to calculate standard deviation of random set (D). Both these metrics indicate the variability as well as stability in boundaries delineated by different experts. Adapted with permission from Kohli et al. (2016).

5. Evaluate and communicate the impact of training data error

Due to the wide range of remote sensing research currently underway, a wide variety of TD and classification algorithms are in use. Therefore, it is not possible to specify a single protocol for

treatment of TD error. Instead, we outline three tiers that represent different levels of accounting for the impact of TD errors on resulting map products.

Tier 1

The optimal TD accuracy assessment, termed Tier 1, involves comparing TD to gold standard training reference data, representing truth. While the term 'truth' may entail an essentially unattainable standard of universal veracity, we suggest that expert consensus, as discussed above, provides a practical benchmark, as well as defining an upper bound on the knowable map accuracy. Using such training reference data, researchers can quantify TD error directly, and thus incorporate it in estimates of output map variance and bias, for example using methods presented by McRoberts et al. [41]. For quantitative variables in which there are substantial TD errors, we recommend the use of type 2 regression, which considers error in both the remotely sensed measurement and the TD, as opposed to type 1 regression, which ignores potential error in the TD. Alternatively, absent such an error metric that explicitly factors training error into its formula, the impact of these errors can be quantified by repeatedly training the model with training datasets adjusted to represent the distributions of measured errors within the training sample, and quantify the resulting differences in the final map accuracy metrics (as in the cropland case study, section 3.3). This approach is likely the most useful in cases where TD are taken from large, pre-existing stock or benchmark libraries.

Tier 2

If it is not possible to directly measure and quantify error in TD, the next best course of action is to introduce a plausible range of simulated error into TD and evaluate its impact on the accuracy of maps trained with these perturbed datasets. If multiple workers are tasked with collecting TD for the same site, then the variance in their data can be used to estimate the uncertainty bounds (e.g. Figure 12). This approach is illustrated in the building mapping case study (section 3.1.1), which illustrates the sensitivity of key accuracy metrics to two different kinds of simulated labelling errors. The wheat yield case study (see section 3.3) provides an example of this approach for a continuous variable. Benchmark datasets may help facilitate this type of training error impact analysis, by providing a common set of training labels with known characteristics that can be systematically modified.

Tier 3

The bare minimum practice for training error accounting should be for researchers to release their training dataset with publication, assuming it is not an existing published dataset, as has been previously recommended (Stehman and Foody, 2019) and sometimes done for reference data [e.g., 50]. These data should be documented with standard metadata, as shown in Table S2, and should also contain a description of the potential uncertainties associated with it. For example, the SpatioTemporal Asset Catalog (STAC) provides a framework for standardization of metadata for EO data and is increasingly seen as an international standard for geospatial data. Additionally, we recommend that researchers use and present the relevant accuracy measure, determined by the study design and goals, and describe clearly that the reported accuracy is itself uncertain, due to possible errors in both training and reference data. These steps allow for scientific replication of research and would also help build an extensive TD repository.

Communication of training data error

Finally, uncertainty that has propagated through the analysis from training data should be faithfully reported in any reporting documentation and maps. We advise researchers to clearly communicate the consequences of TD error and map accuracy, which is becoming more important as EO information products are increasingly used by the public and policy domains. Incomplete error reporting serves to limit the scientific validity and usefulness of these products [45].

It is critical to consider the map's intended audience in order to present uncertainty as clearly and usefully as possible. While we advise always providing full accounting for error sources along with the final accuracy metrics and qualification, it is worth considering carefully how this critical information could best be crafted and presented such that non-specialist audiences will be able to understand the map and its limitations. In general, we recommend including the error on or as close to the actual map whenever possible, whether by means of metrics, the error matrix, and/or by using cartographic techniques for representing uncertainty. Examples of effective cartographic techniques for conveying uncertainty include selection of appropriate, intuitive, and color-blind friendly color schemes for classes and symbols, varying color value and saturation and font/line weight to indicate levels of uncertainty, use of crisp versus blurred boundaries and symbols to indicate the range of uncertainty, or display of consensus maps or side-by-side juxtaposition in cases of multiple, mutually exclusive predictions for the same place and time (e.g. representing differently specified models) [37,38]. Maps of consensus of training polygons and output classes or segments can provide valuable uncertainty information to users, such as shown in Figure 12A-B.

Towards an Open Training Data Repository

For the scientific community, the ideal standard of openness and replicability is to provide a complete description of TD collection practices, appropriate accuracy metrics, and perhaps most importantly of all, the raw data. Ideally, we recommend the creation of a centralized, open source database of all available and relevant training data, using the details collected in the proposed template (Table S2), and drawing inspiration from projects such as STAC. This type of open repository, taking inspiration from similar large-scale databases for computer vision [ImageNet, 167, SIFT10M Dataset, 168], and remote sensing [DeepSat, 169, UC Merced Land Use Dataset, 170], should contain full training metadata, citations to the peer-reviewed literature, as well as links to downloadable versions of TD collection protocols. Following the philosophy of free and open source software, we strongly recommend that researchers embrace open source data, which is the only way by which a study can be truly reproduced.

5. Conclusions

The current treatment of TD in remote sensing research is insufficient for the purposes of reproducibility, uncertainty estimation, and communication of results. This is particularly problematic for error propagation to higher level information products, in which error originating in supposedly gold standard TD may have difficult to predict effects. The purpose of this paper is to call attention to this issue and promote the recommendations outlined above.

It is important to distinguish between the types of 'truth' data that may be used during an EO based mapping project. Here, we refer to four categories of such data: training, validation, training reference and map reference data, of which the latter has the most stringent sampling design requirements [33,66]. The independence of map reference data must be preserved, meaning that whether or not it is collected simultaneously with TD, it must be reserved for final map accuracy analysis. Any data used to enhance or develop ML model parameters (i.e. both training and validation data), must be treated separately from map reference data. In general, our advice is applicable to both map reference and TD, but our recommendations specifically focus on the latter. For a comprehensive review of protocols for reference data collection, we refer the reader to Stehman and Foody [45].

To account for error in TD, we recommend the following steps. Researchers should carefully consider the tolerable levels of error in the desired map before collecting or creating training or reference data. This exercise involves translating the needs of the map users into quantifiably comparable metrics and will guide the selection of these metrics. Next, we recommend that researchers strive to minimize error originating from both design- and collection-related errors; these include appropriate legend definition and imagery selection based on spatial resolution, spatiotemporal representativeness, consensus-based labeling strategies, and interactive feedback to interpreters regarding accuracy. Because it is not possible to completely eliminate TD error, we

strongly advise that such error is incorporated in model outputs, either directly in bias and variance estimates or, if such incorporation is not possible, by documenting the sources and implications of error. As a minimum standard, TD should be fully documented and should be made openly available, allowing others to replicate and assess its use. To guide researchers in this process, we have proposed three tiers of TD error accounting standards, which we believe provide a common basis for comparison of the ability to account for TD error. Finally, we advise that researchers strive to clearly communicate the magnitude and impacts of TD error on map outputs, with specific consideration to the intended or likely audience and users of the map.

Acknowledgements

This work is a synthesis of findings from a workshop held at Clark University on January 8-9, 2019. The workshop and subsequent paper writing and development was supported by a grant from Omidyar Network. Additional support for developing methods and data presented here was provided by NASA (80NSSC18K0158), the National Science Foundation (SES-1801251), National Institute of Standards and Technology (2017-67003-26615), National Institute of Standards and Technology Summer Undergraduate Research Fellowship Program, and New York State Department of Environmental Conservation (DEC01-T00640GG-3350000). We thank Victoria Gammino for helpful input and advice, and David Allen, Ayo Deas, Lucy Hutyra, Clare Kohler, Barry Logan, Jaret Reblin, Ian Smith for assistance with fieldwork and data compilation.

Supplementary Materials

In this problem, TC-based RMSE estimates at each pixel were used to compute a priori probability (P_i) of selecting a particular dataset:

$$P_i = \frac{\frac{1}{\sigma_{\varepsilon_i}^2}}{\sum_{i=1}^{3} \frac{1}{\sigma_{\varepsilon_i}^2}} \quad \text{(S2)}$$

P_i is the probability of selecting measurement system i, $\sigma_{\varepsilon i}$ is the standard deviation of the random error in measurement system i.

Figure S1 depicts how X_T (the training time series for a pixel) is formed by sampling from X_1, X_2, and X_3 over time.

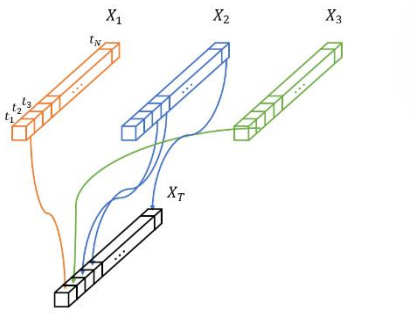

Figure S1: Schematic of product selection using the Triple Collocation approach.

Table S1 shows quantitative results of comparing each of the three models trained for the road detection case in Kumasi, Ghana to the validation labels. This region (shown in Figure 9) included 5,406,942 road pixels and 50,627,010 background pixels.

Table S1: Performance metrics of different models in Kumasi, Ghana

	F1	**IOU**	**Precision**	**Recall**
Khartoum Model				
Average	0.6659	0.5723	0.7758	0.6267
Road	0.3780	0.2330	0.6250	0.2709
Background	0.9538	0.9116	0.9266	0.9862
Kumasi Model				
Average	0.8004	0.6955	0.7693	0.8450
Road	0.6458	0.4769	0.5662	0.7513
Background	0.9552	0.9142	0.9725	0.9386
Khartoum Model retrained in Kumasi				
Average	0.7869	0.6830	0.7965	0.7780
Road	0.6135	0.4425	0.6363	0.5921
Background	0.9603	0.9236	0.9568	0.9639

Table S2: Template and procedure for documenting training data. Note that the 'values' column is intentionally left blank, as this is merely an example. We would expect a fully filled out table to be several pages in length due to the technical nature of the metadata explanation.

Metadata Category	**Value**
Training data set name	
How data were created (technical details, to include number of analysts, whether *in situ* or image interpretation, samples of field sheets, copies of materials used to educate analysts, date of data creation, etc.)	
Funding source	
Purpose	
LULC definitions	

Time period	
Spatial extent	
Spatial resolution (image, field, quadrat, point location)	
Image ID (sensor specific unique identification information)	

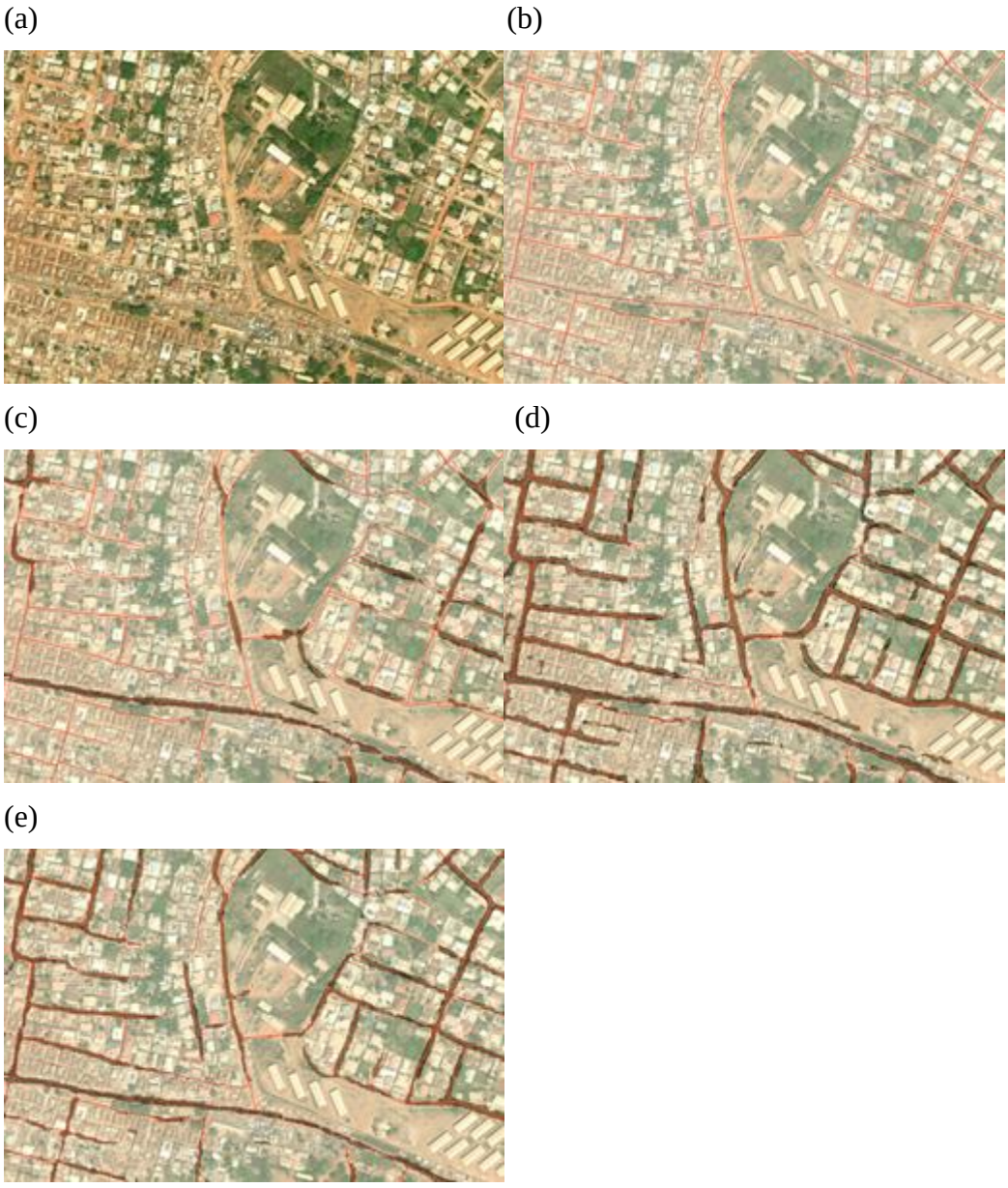

Figure S2: Sample prediction results in Kumasi, Ghana. (a) Input imagery. (b) Predictions from the Las Vegas model. (c) Predictions from the Khartoum model. (d) Prediction from the Kumasi model. (e) Predictions from the Khartoum Model retrained in Kumasi. [In panel b-e model predictions are in shaded color overlaid with validation labels in red on top of imagery.]

Figure S2 shows a qualitative comparison of different model outputs along with the validation labels over a sample area of Figure 4.

References

1. Chen, J.; Chen, J.; Liao, A.; Cao, X.; Chen, L.; Chen, X.; He, C.; Han, G.; Peng, S.; Lu, M.; et al. Global Land Cover Mapping at 30 m Resolution: A POK-Based Operational Approach. *ISPRS J. Photogramm. Remote Sens.* **2015**, *103*, 7–27.
2. Friedl, M.A.; Sulla-Menashe, D.; Tan, B.; Schneider, A.; Ramankutty, N.; Sibley, A.; Huang, X. MODIS Collection 5 global land cover: Algorithm refinements and characterization of new datasets. *Remote Sens. Environ.* **2010**, *114*, 168–182.
3. Song, X.-P.; Hansen, M.C.; Stehman, S.V.; Potapov, P.V.; Tyukavina, A.; Vermote, E.F.; Townshend, J.R. Global land change from 1982 to 2016. *Nature* **2018**, *560*, 639–643.
4. Mohanty, B.P.; Cosh, M.H.; Lakshmi, V.; Montzka, C. Soil Moisture Remote Sensing: State-of-the-Science. *Vadose Zone J.* **2017**, *16*.
5. Daudt, R.C.; Le Saux, B.; Boulch, A.; Gousseau, Y. Guided Anisotropic Diffusion and Iterative Learning for Weakly Supervised Change Detection. *arXiv [cs.CV]* 2019.
6. Hecht, R.; Meinel, G.; Buchroithner, M. Automatic identification of building types based on topographic databases – a comparison of different data sources. *International Journal of Cartography* **2015**, *1*, 18–31.
7. Zhang, X.; Jayavelu, S.; Liu, L.; Friedl, M.A.; Henebry, G.M.; Liu, Y.; Schaaf, C.B.; Richardson, A.D.; Gray, J. Evaluation of land surface phenology from VIIRS data using time series of PhenoCam imagery. *Agric. For. Meteorol.* **2018**, *256-257*, 137–149.
8. Tan, B.; Morisette, J.T.; Wolfe, R.E.; Gao, F.; Ederer, G.A.; Nightingale, J.; Pedelty, J.A. An Enhanced TIMESAT Algorithm for Estimating Vegetation Phenology Metrics From MODIS Data. *IEEE Journal of Selected Topics in Applied Earth Observations and Remote Sensing* **2011**, *4*, 361–371.
9. Zhang, X.; Friedl, M.A.; Schaaf, C.B. Global vegetation phenology from Moderate Resolution Imaging Spectroradiometer (MODIS): Evaluation of global patterns and comparison with in situ measurements: GLOBAL PHENOLOGY FROM MODIS. *J. Geophys. Res.* **2006**, *111*, 981.
10. Wan, Z. New refinements and validation of the MODIS Land-Surface Temperature/Emissivity products. *Remote Sens. Environ.* **2008**, *112*, 59–74.
11. Jiménez-Muñoz, J.C.; Sobrino, J.A.; Skoković, D.; Mattar, C.; Cristóbal, J. Land Surface Temperature Retrieval Methods From Landsat-8 Thermal Infrared Sensor Data. *IEEE Geoscience and Remote Sensing Letters* **2014**, *11*, 1840–1843.
12. Jean, N.; Burke, M.; Xie, M.; Davis, W.M.; Lobell, D.B.; Ermon, S. Combining satellite imagery and machine learning to predict poverty. *Science* **2016**, *353*, 790–794.
13. Pekel, J.-F.; Cottam, A.; Gorelick, N.; Belward, A.S. High-resolution mapping of global surface water and its long-term changes. *Nature* **2016**, *540*, 418–422.
14. Hansen, M.C.; Potapov, P.; Tyukavina, A. Comment on "Tropical forests are a net carbon source based on aboveground measurements of gain and loss." *Science* **2019**, *363*.
15. Gutierrez-Velez, V.H.; Pontius, R.G. Influence of carbon mapping and land change modelling on the prediction of carbon emissions from deforestation. *Environ. Conserv.* **2012**, *39*, 325–336.
16. Loveland, T.R.; Reed, B.C.; Brown, J.F.; Ohlen, D.O.; Zhu, Z.; Yang, L.; Merchant, J.W. Development of a global land cover characteristics database and IGBP DISCover from 1 km AVHRR data. *Int. J. Remote Sens.* **2000**, *21*, 1303–1330.
17. Deng, J.; Dong, W.; Socher, R.; Li, L.-J.; Li, K.; Fei-Fei, L. Imagenet: A large-scale hierarchical image database. In Proceedings of the 2009 IEEE conference on computer vision and pattern recognition; Ieee, 2009; pp. 248–255.
18. Helber, P.; Bischke, B.; Dengel, A.; Borth, D. EuroSAT: A Novel Dataset and Deep Learning Benchmark for Land Use and Land Cover Classification. *IEEE Journal of Selected Topics in Applied Earth Observations and Remote Sensing* **2019**, 1–10.
19. Liu, Q.; Hang, R.; Song, H.; Li, Z. Learning Multiscale Deep Features for High-Resolution Satellite Image Scene Classification. *IEEE Trans. Geosci. Remote Sens.* **2018**, *56*, 117–126.
20. Laso Bayas, J.C.; Lesiv, M.; Waldner, F.; Schucknecht, A.; Duerauer, M.; See, L.; Fritz, S.; Fraisl, D.; Moorthy, I.; McCallum, I.; et al. A global reference database of crowdsourced cropland data collected using the Geo-Wiki platform. *Sci Data* **2017**, *4*, 170136.

21. Lary, D.J.; Zewdie, G.K.; Liu, X.; Wu, D.; Levetin, E.; Allee, R.J.; Malakar, N.; Walker, A.; Mussa, H.; Mannino, A.; et al. Machine Learning Applications for Earth Observation. In *Earth Observation Open Science and Innovation*; Mathieu, P.-P., Aubrecht, C., Eds.; Springer International Publishing: Cham, 2018; pp. 165–218 ISBN 9783319656335.
22. Fortier, J.; Rogan, J.; Woodcock, C.E.; Runfola, D.M. Utilizing Temporally Invariant Calibration Sites to Classify Multiple Dates and Types of Satellite Imagery. *Photogrammetric Engineering & Remote Sensing* **2011**, *77*, 181–189.
23. Foody, G.M.; Mathur, A. Toward intelligent training of supervised image classifications: directing training data acquisition for SVM classification. *Remote Sens. Environ.* **2004**, *93*, 107–117.
24. Graves, S.J.; Asner, G.P.; Martin, R.E.; Anderson, C.B.; Colgan, M.S.; Kalantari, L.; Bohlman, S.A. Tree Species Abundance Predictions in a Tropical Agricultural Landscape with a Supervised Classification Model and Imbalanced Data. *Remote Sensing* **2016**, *8*, 161.
25. Foody, G.; Pal, M.; Rocchini, D.; Garzon-Lopez, C. The sensitivity of mapping methods to reference data quality: Training supervised image classifications with imperfect reference data. *International Journal of …* **2016**.
26. Maxwell, A.E.; Warner, T.A.; Fang, F. Implementation of machine-learning classification in remote sensing: an applied review. *Int. J. Remote Sens.* **2018**, *39*, 2784–2817.
27. Huang, C.; Davis, L.S.; Townshend, J.R.G. An assessment of support vector machines for land cover classification. *Int. J. Remote Sens.* **2002**, *23*, 725–749.
28. Estes, L.; Chen, P.; Debats, S.; Evans, T.; Ferreira, S.; Kuemmerle, T.; Ragazzo, G.; Sheffield, J.; Wolf, A.; Wood, E.; et al. A large-area, spatially continuous assessment of land cover map error and its impact on downstream analyses. *Glob. Chang. Biol.* **2018**, *24*, 322–337.
29. Pengra, B.W.; Stehman, S.V.; Horton, J.A.; Dockter, D.J.; Schroeder, T.A.; Yang, Z.; Cohen, W.B.; Healey, S.P.; Loveland, T.R. Quality control and assessment of interpreter consistency of annual land cover reference data in an operational national monitoring program. *Remote Sens. Environ.* **2019**, 111261.
30. Zhu, X.X.; Tuia, D.; Mou, L.; Xia, G.; Zhang, L.; Xu, F.; Fraundorfer, F. Deep Learning in Remote Sensing: A Comprehensive Review and List of Resources. *IEEE Geoscience and Remote Sensing Magazine* **2017**, *5*, 8–36.
31. Ma, L.; Liu, Y.; Zhang, X.; Ye, Y.; Yin, G.; Johnson, B.A. Deep learning in remote sensing applications: A meta-analysis and review. *ISPRS J. Photogramm. Remote Sens.* **2019**, *152*, 166–177.
32. Foody, G.M. Status of land cover classification accuracy assessment. *Remote Sens. Environ.* **2002**, *80*, 185–201.
33. Foody, G.M. Assessing the accuracy of land cover change with imperfect ground reference data. *Remote Sensing of Environment* 2010, *114*, 2271–2285.
34. Olofsson, P.; Foody, G.M.; Herold, M.; Stehman, S.V.; Woodcock, C.E.; Wulder, M.A. Good practices for estimating area and assessing accuracy of land change. *Remote Sens. Environ.* **2014**, *148*, 42–57.
35. Pontius, R.G.; Millones, M. Death to Kappa: birth of quantity disagreement and allocation disagreement for accuracy assessment. *Int. J. Remote Sens.* **2011**, *32*, 4407–4429.
36. Congalton, R.G.; Green, K. *Assessing the accuracy of remotely sensed data: principles and practices*; CRC press, 2008;.
37. Monmonier, M. Cartography: uncertainty, interventions, and dynamic display. *Prog. Hum. Geogr.* **2006**, *30*, 373–381.
38. MacEachren, A.M. Visualizing Uncertain Information. *1* **1992**, 10–19.
39. Goodchild, M.F.; Gopal, S. *The Accuracy Of Spatial Databases*; CRC Press, 1989; ISBN 9780203490235.
40. Congalton, R.G. A review of assessing the accuracy of classifications of remotely sensed data. *Remote Sens. Environ.* **1991**, *37*, 35–46.
41. McRoberts, R.E.; Stehman, S.V.; Liknes, G.C.; Næsset, E.; Sannier, C.; Walters, B.F. The effects of imperfect reference data on remote sensing-assisted estimators of land cover class proportions. *ISPRS J. Photogramm. Remote Sens.* **2018**, *142*, 292–300.
42. Carlotto, M.J. Effect of errors in ground truth on classification accuracy. *Int. J. Remote Sens.* **2009**, *30*, 4831–4849.

43. Franklin, J.; Simons, D.K.; Beardsley, D.; Rogan, J.M.; Gordon, H. Evaluating Errors in a Digital Vegetation Map with Forest Inventory Data and Accuracy Assessment Using Fuzzy Sets. *Trans. GIS* **2001**, *5*, 285–304.
44. Fritz, S.; See, L.; McCallum, I.; Schill, C.; Obersteiner, M.; van der Velde, M.; Boettcher, H.; Havlík, P.; Achard, F. Highlighting continued uncertainty in global land cover maps for the user community. *Environmental Research Letters* 2011, *6*, 044005.
45. Stehman, S.V.; Foody, G.M. Key issues in rigorous accuracy assessment of land cover products. *Remote Sens. Environ.* **2019**, *231*, 111199.
46. Copass, C.; Antonova, N.; Kennedy, R. Comparison of Office and Field Techniques for Validating Landscape Change Classification in Pacific Northwest National Parks. *Remote Sensing* **2018**, *11*, 3.
47. Lesiv, M.; See, L.; Laso Bayas, J.C.; Sturn, T.; Schepaschenko, D.; Karner, M.; Moorthy, I.; McCallum, I.; Fritz, S. Characterizing the Spatial and Temporal Availability of Very High Resolution Satellite Imagery in Google Earth and Microsoft Bing Maps as a Source of Reference Data. *Land* **2018**, *7*, 118.
48. Biradar, C.M.; Thenkabail, P.S.; Noojipady, P.; Li, Y.; Dheeravath, V.; Turral, H.; Velpuri, M.; Gumma, M.K.; Gangalakunta, O.R.P.; Cai, X.L.; et al. A global map of rainfed cropland areas (GMRCA) at the end of last millennium using remote sensing. *Int. J. Appl. Earth Obs. Geoinf.* **2009**, *11*, 114–129.
49. Sulla-Menashe, D.; Gray, J.M.; Abercrombie, S.P.; Friedl, M.A. Hierarchical mapping of annual global land cover 2001 to present: The MODIS Collection 6 Land Cover product. *Remote Sens. Environ.* **2019**, *222*, 183–194.
50. Xiong, J.; Thenkabail, P.S.; Tilton, J.C.; Gumma, M.K.; Teluguntla, P.; Oliphant, A.; Congalton, R.G.; Yadav, K.; Gorelick, N. Nominal 30-m Cropland Extent Map of Continental Africa by Integrating Pixel-Based and Object-Based Algorithms Using Sentinel-2 and Landsat-8 Data on Google Earth Engine. *Remote Sensing* **2017**, *9*, 1065.
51. Mallinis, G.; Emmanoloudis, D.; Giannakopoulos, V.; Maris, F.; Koutsias, N. Mapping and interpreting historical land cover/land use changes in a Natura 2000 site using earth observational data: The case of Nestos delta, Greece. *Appl. Geogr.* **2011**, *31*, 312–320.
52. Jawak, S.D.; Luis, A.J. Improved land cover mapping using high resolution multiangle 8-band WorldView-2 satellite remote sensing data. *JARS* **2013**, *7*, 073573.
53. Ye, S.; Pontius, R.G.; Rakshit, R. A review of accuracy assessment for object-based image analysis: From per-pixel to per-polygon approaches. *ISPRS J. Photogramm. Remote Sens.* **2018**, *141*, 137–147.
54. Fritz, S.; See, L.; Perger, C.; McCallum, I.; Schill, C.; Schepaschenko, D.; Duerauer, M.; Karner, M.; Dresel, C.; Laso-Bayas, J.-C.; et al. A global dataset of crowdsourced land cover and land use reference data. *Sci Data* **2017**, *4*, 170075.
55. Stehman, S.V. Sampling designs for accuracy assessment of land cover. *Int. J. Remote Sens.* **2009**, *30*, 5243–5272.
56. Brodrick, P.G.; Davies, A.B.; Asner, G.P. Uncovering Ecological Patterns with Convolutional Neural Networks. *Trends Ecol. Evol.* **2019**, *34*, 734–745.
57. Xiao, T.; Xia, T.; Yang, Y.; Huang, C.; Wang, X. Learning from massive noisy labeled data for image classification. In Proceedings of the Proceedings of the IEEE conference on computer vision and pattern recognition; cv-foundation.org, 2015; pp. 2691–2699.
58. Frénay, B.; Verleysen, M. Classification in the presence of label noise: a survey. *IEEE Trans Neural Netw Learn Syst* **2014**, *25*, 845–869.
59. Brodley, C.E.; Friedl, M.A. Identifying Mislabeled Training Data. *1* **1999**, *11*, 131–167.
60. Van Etten, A.; Lindenbaum, D.; Bacastow, T.M. SpaceNet: A Remote Sensing Dataset and Challenge Series. *arXiv [cs.CV]* 2018.
61. Sumbul, G.; Charfuelan, M.; Demir, B.; Markl, V. BigEarthNet: A Large-Scale Benchmark Archive For Remote Sensing Image Understanding. *arXiv [cs.CV]* 2019.
62. Lesiv, M.; Laso Bayas, J.C.; See, L.; Duerauer, M.; Dahlia, D.; Durando, N.; Hazarika, R.; Kumar Sahariah, P.; Vakolyuk, M. 'yana; Blyshchyk, V.; et al. Estimating the global distribution of field size using crowdsourcing. *Glob. Chang. Biol.* **2019**, *25*, 174–186.
63. Fritz, S.; McCallum, I.; Schill, C.; Perger, C.; See, L.; Schepaschenko, D.; van der Velde, M.; Kraxner, F.; Obersteiner, M. Geo-Wiki: An Online Platform for Improving Global Land

Cover. *Environmental Modelling & Software* **2012**, *31*, 110–123.
64. Goodchild, M.F. Citizens as sensors: the world of volunteered geography. *GeoJournal* **2007**, *69*, 211–221.
65. Kohavi, R.; Others A study of cross-validation and bootstrap for accuracy estimation and model selection. In Proceedings of the Ijcai; Montreal, Canada, 1995; Vol. 14, pp. 1137–1145.
66. Olofsson, P.; Foody, G.M.; Stehman, S.V.; Woodcock, C.E. Making better use of accuracy data in land change studies: Estimating accuracy and area and quantifying uncertainty using stratified estimation. *Remote Sens. Environ.* **2013**, *129*, 122–131.
67. Stehman, S.V.; Czaplewski, R.L. Design and Analysis for Thematic Map Accuracy Assessment: Fundamental Principles. *Remote Sens. Environ.* **1998**, *64*, 331–344.
68. Stehman, S.V. Practical Implications of Design-Based Sampling Inference for Thematic Map Accuracy Assessment. *Remote Sens. Environ.* **2000**, *72*, 35–45.
69. Kuzera, K.; Pontius, R.G. Importance of Matrix Construction for Multiple-Resolution Categorical Map Comparison. *GISci. Remote Sens.* **2008**, *45*, 249–274.
70. Pontius, R.G.; Thontteh, O.; Chen, H. Components of information for multiple resolution comparison between maps that share a real variable. *Environ. Ecol. Stat.* **2008**, *15*, 111–142.
71. Pontius, R.G.; Parmentier, B. Recommendations for using the relative operating characteristic (ROC). *Landsc. Ecol.* **2014**, *29*, 367–382.
72. Pontius, R.G. Component intensities to relate difference by category with difference overall. *Int. J. Appl. Earth Obs. Geoinf.* **2019**, *77*, 94–99.
73. Pontius, R.G., Jr.; Connors, J. Range of Categorical Associations for Comparison of Maps with Mixed Pixels. *Photogrammetric Engineering & Remote Sensing* **2009**, *75*, 963–969.
74. Aldwaik, S.Z.; Pontius, R.G., Jr. Intensity analysis to unify measurements of size and stationarity of land changes by interval, category, and transition. *Landsc. Urban Plan.* **2012**, *106*, 103–114.
75. Pontius, R.G.; Gao, Y.; Giner, N.M.; Kohyama, T.; Osaki, M.; Hirose, K. Design and Interpretation of Intensity Analysis Illustrated by Land Change in Central Kalimantan, Indonesia. *Land* **2013**, *2*, 351–369.
76. Foody, G.M. Harshness in image classification accuracy assessment. *Int. J. Remote Sens.* **2008**, *29*, 3137–3158.
77. Cohen, J. A Coefficient of Agreement for Nominal Scales. *Educ. Psychol. Meas.* **1960**, *20*, 37–46.
78. Allouche, O.; Tsoar, A.; Kadmon, R. Assessing the Accuracy of Species Distribution Models: Prevalence, Kappa and the True Skill Statistic (TSS). *J. Appl. Ecol.* **2006**, *43*, 1223–1232.
79. Blaschke, T. Object based image analysis for remote sensing. *ISPRS J. Photogramm. Remote Sens.* **2010**, *65*, 2–16.
80. Zhang, Q.-M.; Shang, M.-S.; Zeng, W.; Chen, Y.; Lü, L. Empirical comparison of local structural similarity indices for collaborative-filtering-based recommender systems. *Phys. Procedia* **2010**, *3*, 1887–1896.
81. Marçal, A.R.S.; Rodrigues, A.S. A method for multi-spectral image segmentation evaluation based on synthetic images. *Comput. Geosci.* **2009**, *35*, 1574–1581.
82. Rahman, M.A.; Wang, Y. Optimizing Intersection-Over-Union in Deep Neural Networks for Image Segmentation. In Proceedings of the Advances in Visual Computing; Springer International Publishing, 2016; pp. 234–244.
83. Shi, R.; Ngan, K.N.; Li, S. Jaccard index compensation for object segmentation evaluation. In Proceedings of the 2014 IEEE International Conference on Image Processing (ICIP); 2014; pp. 4457–4461.
84. Willmott, C.J.; Matsuura, K. On the use of dimensioned measures of error to evaluate the performance of spatial interpolators. *Int. J. Geogr. Inf. Sci.* **2006**, *20*, 89–102.
85. Willmott, C.J.; Matsuura, K.; Robeson, S.M. Ambiguities inherent in sums-of-squares-based error statistics. *Atmos. Environ.* **2009**, *43*, 749–752.
86. Willmott, C.J.; Matsuura, K. Advantages of the mean absolute error (MAE) over the root mean square error (RMSE) in assessing average model performance. *Clim. Res.* **2005**, *30*, 79–82.
87. Pontius, R.G., Jr; Si, K. The total operating characteristic to measure diagnostic ability for multiple thresholds. *Int. J. Geogr. Inf. Sci.* **2014**, *28*, 570–583.
88. Fielding, A.H.; Bell, J.F. A review of methods for the assessment of prediction errors in

conservation presence/absence models. *Environ. Conserv.* **1997**, *24*, 38–49.
89. Foody, G.M. Ground reference data error and the mis-estimation of the area of land cover change as a function of its abundance. *Remote Sens. Lett.* **2013**, *4*, 783–792.
90. Powell, R.L.; Matzke, N.; de Souza, C.; Clark, M.; Numata, I.; Hess, L.L.; Roberts, D.A. Sources of error in accuracy assessment of thematic land-cover maps in the Brazilian Amazon. *Remote Sens. Environ.* **2004**, *90*, 221–234.
91. Clark, M.L.; Aide, T.M.; Riner, G. Land change for all municipalities in Latin America and the Caribbean assessed from 250-m MODIS imagery (2001–2010). *Remote Sens. Environ.* **2012**, *126*, 84–103.
92. Swan, B.; Laverdiere, M.; Yang, H.L. How Good is Good Enough?: Quantifying the Effects of Training Set Quality. In Proceedings of the Proceedings of the 2Nd ACM SIGSPATIAL International Workshop on AI for Geographic Knowledge Discovery; ACM: New York, NY, USA, 2018; pp. 47–51.
93. Planet Team Planet Application Program Interface: In Space for Life on Earth. San Francisco, CA 2017.
94. Manfreda, S.; McCabe, M.F.; Miller, P.E.; Lucas, R.; Pajuelo Madrigal, V.; Mallinis, G.; Ben Dor, E.; Helman, D.; Estes, L.; Ciraolo, G.; et al. On the Use of Unmanned Aerial Systems for Environmental Monitoring. *Remote Sensing* **2018**, *10*, 641.
95. Toutin, T. Geometric processing of IKONOS Geo images with DEM. In Proceedings of the Proceedings of ISPRS Joint Workshop "High Resolution Mapping from Space" 2001; pdfs.semanticscholar.org, 2001; pp. 19–21.
96. Reinartz, P.; Müller, R.; Schwind, P.; Suri, S.; Bamler, R. Orthorectification of VHR optical satellite data exploiting the geometric accuracy of TerraSAR-X data. *ISPRS J. Photogramm. Remote Sens.* **2011**, *66*, 124–132.
97. Aguilar, M.A.; Saldaña, M. del M.; Aguilar, F.J. Assessing geometric accuracy of the orthorectification process from GeoEye-1 and WorldView-2 panchromatic images. *Int. J. Appl. Earth Obs. Geoinf.* **2013**, *21*, 427–435.
98. Chen, J.; Zipf, A. DeepVGI: Deep Learning with Volunteered Geographic Information. In Proceedings of the Proceedings of the 26th International Conference on World Wide Web Companion; International World Wide Web Conferences Steering Committee: Republic and Canton of Geneva, Switzerland, 2017; pp. 771–772.
99. Kaiser, P.; Wegner, J.D.; Lucchi, A.; Jaggi, M.; Hofmann, T.; Schindler, K. Learning Aerial Image Segmentation From Online Maps. *IEEE Trans. Geosci. Remote Sens.* **2017**, *55*, 6054–6068.
100. Audebert, N.; Le Saux, B.; Lefèvre, S. Joint learning from earth observation and openstreetmap data to get faster better semantic maps. In Proceedings of the Proceedings of the IEEE Conference on Computer Vision and Pattern Recognition Workshops; 2017; pp. 67–75.
101. Strahler, A.H.; Woodcock, C.E.; Smith, J.A. On the nature of models in remote sensing. *Remote Sens. Environ.* **1986**, *20*, 121–139.
102. Shao, Y.; Lunetta, R.S. Comparison of support vector machine, neural network, and CART algorithms for the land-cover classification using limited training data points. *ISPRS J. Photogramm. Remote Sens.* **2012**, *70*, 78–87.
103. Foody, G.M. Relating the land-cover composition of mixed pixels to artificial neural network classification output. *Photogramm. Eng. Remote Sens.* **1996**, *62*, 491–498.
104. Moody, A.; Gopal, S.; Strahler, A.H. Artificial neural network response to mixed pixels in coarse-resolution satellite data. *Remote Sens. Environ.* **1996**, *58*, 329–343.
105. Oppenshaw, S.; Taylor, P. A million or so correlation coefficients. *Statistical methods in the spatial sciences. Pion, London* **1979**.
106. Jelinski, D.E.; Wu, J. The modifiable areal unit problem and implications for landscape ecology. *Landsc. Ecol.* **1996**, *11*, 129–140.
107. Weiss, M.; de Beaufort, L.; Baret, F.; Allard, D.; Bruguier, N.; Marloie, O. Mapping leaf area index measurements at different scales for the validation of large swath satellite sensors: first results of the VALERI project. In Proceedings of the 8th International symposium in physical measurements and remote sensing, Aussois (France); w3.avignon.inra.fr, 2001; pp. 125–130.
108. Tian, Y.; Woodcock, C.E.; Wang, Y.; Privette, J.L.; Shabanov, N.V.; Zhou, L.; Zhang, Y.;

Buermann, W.; Dong, J.; Veikkanen, B.; et al. Multiscale analysis and validation of the MODIS LAI product: I. Uncertainty assessment. *Remote Sens. Environ.* **2002**, *83*, 414–430.
109. Masuoka, E.; Roy, D.; Wolfe, R.; Morisette, J.; Sinno, S.; Teague, M.; Saleous, N.; Devadiga, S.; Justice, C.O.; Nickeson, J. MODIS Land Data Products: Generation, Quality Assurance and Validation. In *Land Remote Sensing and Global Environmental Change: NASA's Earth Observing System and the Science of ASTER and MODIS*; Ramachandran, B., Justice, C.O., Abrams, M.J., Eds.; Springer New York: New York, NY, 2011; pp. 509–531 ISBN 9781441967497.
110. Cohen, W.B.; Justice, C.O. Validating MODIS terrestrial ecology products: linking in situ and satellite measurements. *Remote Sens. Environ.* **1999**, *70*, 1–3.
111. Fritz, S.; See, L.; McCallum, I.; You, L.; Bun, A.; Moltchanova, E.; Duerauer, M.; Albrecht, F.; Schill, C.; Perger, C.; et al. Mapping global cropland and field size. *Glob. Chang. Biol.* **2015**, *21*, 1980–1992.
112. Debats, S.R.; Estes, L.D.; Thompson, D.R.; Caylor, K.K. *Integrating active learning and crowdsourcing into large-scale supervised landcover mapping algorithms*; PeerJ Preprints, 2017;.
113. Estes, L.D.; McRitchie, D.; Choi, J.; Debats, S.; Evans, T.; Guthe, W.; Luo, D.; Ragazzo, G.; Zempleni, R.; Caylor, K.K. A Platform for Crowdsourcing the Creation of Representative, Accurate Landcover Maps. *Environmental Modelling & Software* **2016**, *80*, 41–53.
114. Waldner, F.; Schucknecht, A.; Lesiv, M.; Gallego, J.; See, L.; Pérez-Hoyos, A.; d'Andrimont, R.; de Maet, T.; Bayas, J.C.L.; Fritz, S.; et al. Conflation of expert and crowd reference data to validate global binary thematic maps. *Remote Sens. Environ.* **2019**, *221*, 235–246.
115. Bey, A.; Sánchez-Paus Díaz, A.; Maniatis, D.; Marchi, G.; Mollicone, D.; Ricci, S.; Bastin, J.-F.; Moore, R.; Federici, S.; Rezende, M.; et al. Collect Earth: Land Use and Land Cover Assessment through Augmented Visual Interpretation. *Remote Sensing* **2016**, *8*, 807.
116. Fritz, S.; Sturn, T.; Karner, M.; Moorthy, I.; See, L.; Laso Bayas, J.C.; Fraisl, D. FotoQuest Go: A Citizen Science Approach to the Collection of In-Situ Land Cover and Land Use Data for Calibration and Validation.; pure.iiasa.ac.at, 2019.
117. Tuia, D.; Pasolli, E.; Emery, W.J. Using active learning to adapt remote sensing image classifiers. *Remote Sensing of Environment* 2011, *115*, 2232–2242.
118. Neigh, C.S.R.; Carroll, M.L.; Wooten, M.R.; McCarty, J.L.; Powell, B.F.; Husak, G.J.; Enenkel, M.; Hain, C.R. Smallholder crop area mapped with wall-to-wall WorldView sub-meter panchromatic image texture: A test case for Tigray, Ethiopia. *Remote Sens. Environ.* **2018**, *212*, 8–20.
119. Comber, A.; Fisher, P. What is land cover? *Environment and Planning* **2005**.
120. Kohli, D.; Sliuzas, R.; Kerle, N.; Stein, A. An ontology of slums for image-based classification. *Comput. Environ. Urban Syst.* **2012**, *36*, 154–163.
121. Verburg, P.H.; Neumann, K.; Nol, L. Challenges in using land use and land cover data for global change studies. *Glob. Chang. Biol.* **2011**, *17*, 974–989.
122. Weng, Q. Remote sensing of impervious surfaces in the urban areas: Requirements, methods, and trends. *Remote Sens. Environ.* **2012**, *117*, 34–49.
123. Kohli, D.; Stein, A.; Sliuzas, R. Uncertainty analysis for image interpretations of urban slums. *Comput. Environ. Urban Syst.* **2016**, *60*, 37–49.
124. Rocchini, D. While Boolean sets non-gently rip: A theoretical framework on fuzzy sets for mapping landscape patterns. *Ecol. Complex.* **2010**, *7*, 125–129.
125. Woodcock, C.E.; Gopal, S. Fuzzy set theory and thematic maps: accuracy assessment and area estimation. *Int. J. Geogr. Inf. Sci.* **2000**, *14*, 153–172.
126. Rocchini, D.; Foody, G.M.; Nagendra, H.; Ricotta, C.; Anand, M.; He, K.S.; Amici, V.; Kleinschmit, B.; Förster, M.; Schmidtlein, S.; et al. Uncertainty in ecosystem mapping by remote sensing. *Comput. Geosci.* **2013**, *50*, 128–135.
127. Zhang, J.; Foody, G.M. A fuzzy classification of sub-urban land cover from remotely sensed imagery. *Int. J. Remote Sens.* **1998**, *19*, 2721–2738.
128. Woodcock, C.E.; Strahler, A.H. The factor of scale in remote sensing. *Remote Sens. Environ.* **1987**, *21*, 311–332.
129. Foody, G.M. The continuum of classification fuzziness in thematic mapping. *Photogramm.*

Eng. Remote Sens. **1999**, *65*, 443–452.
130. Tewkesbury, A.P.; Comber, A.J.; Tate, N.J.; Lamb, A.; Fisher, P.F. A critical synthesis of remotely sensed optical image change detection techniques. *Remote Sens. Environ.* **2015**, *160*, 1–14.
131. Stehman, S.V.; Fonte, C.C.; Foody, G.M.; See, L. Using volunteered geographic information (VGI) in design-based statistical inference for area estimation and accuracy assessment of land cover. *Remote Sens. Environ.* **2018**, *212*, 47–59.
132. Thompson, I.D.; Maher, S.C.; Rouillard, D.P.; Fryxell, J.M.; Baker, J.A. Accuracy of forest inventory mapping: Some implications for boreal forest management. *For. Ecol. Manage.* **2007**, *252*, 208–221.
133. Bland, M.J.; Altman, D.G. Statistics notes: Measurement error. *BMJ* **1996**, *312*, 1654.
134. Martin, D. An Introduction to "The Guide to the Expression of Uncertainty in Measurement." In *Evaluation of measurement data -- Guide to the expression of uncertainty in measurement*; JCGM, 2008; pp. 1–10.
135. Foody, G.M. The impact of imperfect ground reference data on the accuracy of land cover change estimation. *Int. J. Remote Sens.* **2009**, *30*, 3275–3281.
136. Multi-Resolution Land Characteristics Consortium (U.S.) National land cover dataset (NLCD).
137. Menon, S.; Akbari, H.; Mahanama, S.; Sednev, I.; Levinson, R. Radiative forcing and temperature response to changes in urban albedos and associated CO2 offsets. *Environ. Res. Lett.* **2010**, *5*, 014005.
138. Hutyra, L.R.; Yoon, B.; Hepinstall-Cymerman, J.; Alberti, M. Carbon consequences of land cover change and expansion of urban lands: A case study in the Seattle metropolitan region. *Landsc. Urban Plan.* **2011**, *103*, 83–93.
139. Reinmann, A.B.; Hutyra, L.R.; Trlica, A.; Olofsson, P. Assessing the global warming potential of human settlement expansion in a mesic temperate landscape from 2005 to 2050. *Sci. Total Environ.* **2016**, *545-546*, 512–524.
140. Hardiman, B.S.; Wang, J.A.; Hutyra, L.R.; Gately, C.K.; Getson, J.M.; Friedl, M.A. Accounting for urban biogenic fluxes in regional carbon budgets. *Sci. Total Environ.* **2017**, *592*, 366–372.
141. Seto, K.C.; Güneralp, B.; Hutyra, L.R. Global forecasts of urban expansion to 2030 and direct impacts on biodiversity and carbon pools. *Proc. Natl. Acad. Sci. U. S. A.* **2012**, *109*, 16083–16088.
142. Angel, S.; Parent, J.; Civco, D.L.; Blei, A.; Potere, D. The dimensions of global urban expansion: Estimates and projections for all countries, 2000–2050. *Prog. Plann.* **2011**, *75*, 53–107.
143. Coulston, J.W.; Moisen, G.G.; Wilson, B.T.; Finco, M.V.; Cohen, W.B.; Brewer, C.K. Modeling percent tree canopy cover: a pilot study. *Photogrammetric Engineering & Remote Sensing 78 (7): 715--727* **2012**, *78*, 715–727.
144. Reinmann, A.B.; Hutyra, L.R. Edge effects enhance carbon uptake and its vulnerability to climate change in temperate broadleaf forests. *Proc. Natl. Acad. Sci. U. S. A.* **2017**, *114*, 107–112.
145. Rolnick, D.; Veit, A.; Belongie, S.; Shavit, N. Deep Learning is Robust to Massive Label Noise. *arXiv [cs.LG]* 2017.
146. Breiman, L. Random Forests. *Mach. Learn.* **2001**, *45*, 5–32.
147. Lyndon D. Estes, Su Ye, Lei Song, Ron Eastman, Sitian Xiong, Tammy Woodard, Boka Luo, Dennis McRitchie, Ryan Avery, Kelly Caylor, Stephanie, Debats. Improving cropland maps through tight integration of human and machine intelligence. *In preparation*.
148. Debats, S.R.; Luo, D.; Estes, L.D.; Fuchs, T.J.; Caylor, K.K. A Generalized Computer Vision Approach to Mapping Crop Fields in Heterogeneous Agricultural Landscapes. *Remote Sens. Environ.* **2016**, *179*, 210–221.
149. Jain, M.; Balwinder-Singh; Rao, P.; Srivastava, A.K.; Poonia, S.; Blesh, J.; Azzari, G.; McDonald, A.J.; Lobell, D.B. The impact of agricultural interventions can be doubled by using satellite data. *Nature Sustainability* **2019**, *2*, 931–934.
150. Pontius, R.G. Criteria to Confirm Models that Simulate Deforestation and Carbon Disturbance. *Land* **2018**, *7*, 105.

151. Waldner, F.; De Abelleyra, D.; Verón, S.R.; Zhang, M.; Wu, B.; Plotnikov, D.; Bartalev, S.; Lavreniuk, M.; Skakun, S.; Kussul, N.; et al. Towards a set of agrosystem-specific cropland mapping methods to address the global cropland diversity. *Int. J. Remote Sens.* **2016**, *37*, 3196–3231.
152. Nachmany, Y.; Alemohammad, H. Detecting Roads from Satellite Imagery in the Developing World. In Proceedings of the Proceedings of the IEEE Conference on Computer Vision and Pattern Recognition Workshops; openaccess.thecvf.com, 2019; pp. 83–89.
153. Castelluccio, M.; Poggi, G.; Sansone, C.; Verdoliva, L. Land Use Classification in Remote Sensing Images by Convolutional Neural Networks. *arXiv [cs.CV]* 2015.
154. Azevedo, T., Sr.; Souza, C.M., Jr.; Shimbo, J.; Alencar, A. MapBiomas initiative: Mapping annual land cover and land use changes in Brazil from 1985 to 2017.; adsabs.harvard.edu, 2018; Vol. 2018.
155. Brown, J.F.; Tollerud, H.J.; Barber, C.P.; Zhou, Q.; Dwyer, J.L.; Vogelmann, J.E.; Loveland, T.R.; Woodcock, C.E.; Stehman, S.V.; Zhu, Z.; et al. Lessons learned implementing an operational continuous United States national land change monitoring capability: The Land Change Monitoring, Assessment, and Projection (LCMAP) approach. *Remote Sens. Environ.* **2019**, 111356.
156. Estes, L.; Elsen, P.R.; Treuer, T.; Ahmed, L.; Caylor, K.; Chang, J.; Choi, J.J.; Ellis, E.C. The spatial and temporal domains of modern ecology. *Nat Ecol Evol* **2018**, *2*, 819–826.
157. Jensen, J.R.; Cowen, D.C. Remote sensing of urban/suburban infrastructure and socio-economic attributes. *Photogramm. Eng. Remote Sens.* **1999**, *65*, 611–622.
158. Rozenstein, O.; Karnieli, A. Comparison of methods for land-use classification incorporating remote sensing and GIS inputs. *Appl. Geogr.* **2011**, *31*, 533–544.
159. Dorais, A.; Cardille, J. Strategies for Incorporating High-Resolution Google Earth Databases to Guide and Validate Classifications: Understanding Deforestation in Borneo. *Remote Sensing* **2011**, *3*, 1157–1176.
160. Sexton, J.O.; Urban, D.L.; Donohue, M.J.; Song, C. Long-term land cover dynamics by multi-temporal classification across the Landsat-5 record. *Remote Sens. Environ.* **2013**, *128*, 246–258.
161. Carletto, C.; Gourlay, S.; Winters, P. From Guesstimates to GPStimates: Land Area Measurement and Implications for Agricultural Analysis. *J. Afr. Econ.* **2015**, *24*, 593–628.
162. Laso Bayas, J.C.; See, L.; Fritz, S.; Sturn, T.; Perger, C.; Dürauer, M.; Karner, M.; Moorthy, I.; Schepaschenko, D.; Domian, D.; et al. Crowdsourcing In-Situ Data on Land Cover and Land Use Using Gamification and Mobile Technology. *Remote Sensing* **2016**, *8*, 905.
163. Burke, M.; Lobell, D.B. Satellite-based assessment of yield variation and its determinants in smallholder African systems. *Proc. Natl. Acad. Sci. U. S. A.* **2017**.
164. Jin, Z.; Azzari, G.; You, C.; Di Tommaso, S.; Aston, S.; Burke, M.; Lobell, D.B. Smallholder maize area and yield mapping at national scales with Google Earth Engine. *Remote Sens. Environ.* **2019**, *228*, 115–128.
165. Lobell, D.B.; Thau, D.; Seifert, C.; Engle, E.; Little, B. A Scalable Satellite-Based Crop Yield Mapper. *Remote Sens. Environ.* **2015**, *164*, 324–333.
166. Grassini, P.; van Bussel, L.G.J.; Van Wart, J.; Wolf, J.; Claessens, L.; Yang, H.; Boogaard, H.; de Groot, H.; van Ittersum, M.K.; Cassman, K.G. How Good Is Good Enough? Data Requirements for Reliable Crop Yield Simulations and Yield-Gap Analysis. *Field Crops Res.* **2015**, *177*, 49–63.
167. Russakovsky, O.; Deng, J.; Su, H.; Krause, J.; Satheesh, S.; Ma, S.; Huang, Z.; Karpathy, A.; Khosla, A.; Bernstein, M.; et al. ImageNet Large Scale Visual Recognition Challenge. *Int. J. Comput. Vis.* **2015**, *115*, 211–252.
168. Fu, X.; McCane, B.; Mills, S.; Albert, M. NOKMeans: Non-Orthogonal K-means Hashing. In *Computer Vision -- ACCV 2014*; Cremers, D., Reid, I., Saito, H., Yang, M.-H., Eds.; Lecture Notes in Computer Science; Springer International Publishing: Cham, 2015; Vol. 9003, pp. 162–177 ISBN 9783319168647.
169. Basu, S.; Ganguly, S.; Mukhopadhyay, S.; DiBiano, R.; Karki, M.; Nemani, R. DeepSat: A Learning Framework for Satellite Imagery. In Proceedings of the Proceedings of the 23rd SIGSPATIAL International Conference on Advances in Geographic Information Systems;

ACM: New York, NY, USA, 2015; pp. 37:1–37:10.
170. Yang, Y.; Newsam, S. Bag-of-visual-words and spatial extensions for land-use classification. *Proceedings of the 18th SIGSPATIAL international* **2010**.